



LAWRENCE  
LIVERMORE  
NATIONAL  
LABORATORY

LLNL-TR-653180

# Beryllium Dynamic Strength Measurements: Report on Task 3 Agreement #B590737

V. V. Igonin

April 15, 2014

## Disclaimer

---

This document was prepared as an account of work sponsored by an agency of the United States government. Neither the United States government nor Lawrence Livermore National Security, LLC, nor any of their employees makes any warranty, expressed or implied, or assumes any legal liability or responsibility for the accuracy, completeness, or usefulness of any information, apparatus, product, or process disclosed, or represents that its use would not infringe privately owned rights. Reference herein to any specific commercial product, process, or service by trade name, trademark, manufacturer, or otherwise does not necessarily constitute or imply its endorsement, recommendation, or favoring by the United States government or Lawrence Livermore National Security, LLC. The views and opinions of authors expressed herein do not necessarily state or reflect those of the United States government or Lawrence Livermore National Security, LLC, and shall not be used for advertising or product endorsement purposes.

This work performed under the auspices of the U.S. Department of Energy by Lawrence Livermore National Laboratory under Contract DE-AC52-07NA27344.



RUSSIAN FEDERAL NUCLEAR CENTER  
All-Russia Research Institute of Experimental Physics  
VNIIEF

## BERYLLIUM DYNAMIC STRENGTH MEASUREMENTS

Report on Task 3  
Agreement # B590737  
between RFNC – VNIIEF (Russia) and LLNS (USA)

Head of works under Agreement

\_\_\_\_\_ V.V. Igonin

2012

2012

## Contents

Introduction .....	3
1 Used techniques .....	4
1.1 Radiographic technique .....	4
1.2 Laser-interferometric technique.....	5
1.3 Manganin technique.....	6
2 Experimental setup .....	7
2.1 Radiographic experiments .....	7
2.2 Experiments with recovery of samples.....	10
2.2.1 Assembly №1. Transition of quasi-isentropic compression wave into SW....	11
2.2.2 Assembly 2. Shock wave loading of decreasing amplitude.....	14
3 Experimental results .....	17
3.1 Roentgenographic experiments .....	17
3.2 Results of measurements via laser interferometer .....	22
3.3 Experiments with recovery of samples.....	26
3.3.1 Test №1 .....	26
3.3.2 Test №2 .....	27
3.4 Results of metallographic investigations.....	28
3.4.1 Technique of metallographic analysis.....	28
3.4.2 Test № 1 .....	29
3.4.3 Test № 2 .....	31
3.4.4 Discussion of results.....	33
4 Relaxation model of beryllium strength (RING) .....	34
4.1 Equations of state.....	34
4.2 Shear modulus and melting temperature .....	36
4.3 Relaxation model RING-I.....	39
5 Results of numerical simulation of experiments with use of Eulerian technique .....	41
6 Results of numerical simulation of experiments by using Lagrangian technique.....	48
Conclusion .....	50
References .....	51

## Introduction

The goal of the work under Agreement #B590737 consisted in the development of the experimentally justified model of beryllium shear strength of American production (*Be S200F*) in the pressure range of  $\sim 10\div 60$  GPa and at strain rates up to  $\dot{\epsilon}_i \approx 10^6 \text{ s}^{-1}$ . The *Be* shear strength models, which were available in this range of parameters, had no sufficiently reliable experimental justification.

The purpose of the third final phase consisted in the performance of tests by using the method of perturbations and with recovery of samples *Be S200F* and parametric verification of a model of beryllium strength on their basis.

In the course of the works of the third phase six experiments were performed with the use of the dynamic method of perturbations [1], [2] with shock-free loading of the *Be S200F* samples under investigation up to the pressure  $P_m \approx 50$  GPa. The growth of the specified perturbations was recorded by means of the radiographic technique. In addition, each experiment includes measurements of free surface velocities of a liner by using a laser interferometer of the VISAR type.

Two experiments were implemented with loading of beryllium samples up to the pressure  $P \sim 25\div 60$  GPa with recovery followed by metallographic investigation. The objective of the metallographic investigation consisted of determination of peculiarities of high-rate deformation of *Be*. Measurements were carried out in each experiment by using the technique of a manganin-based pressure sensor.

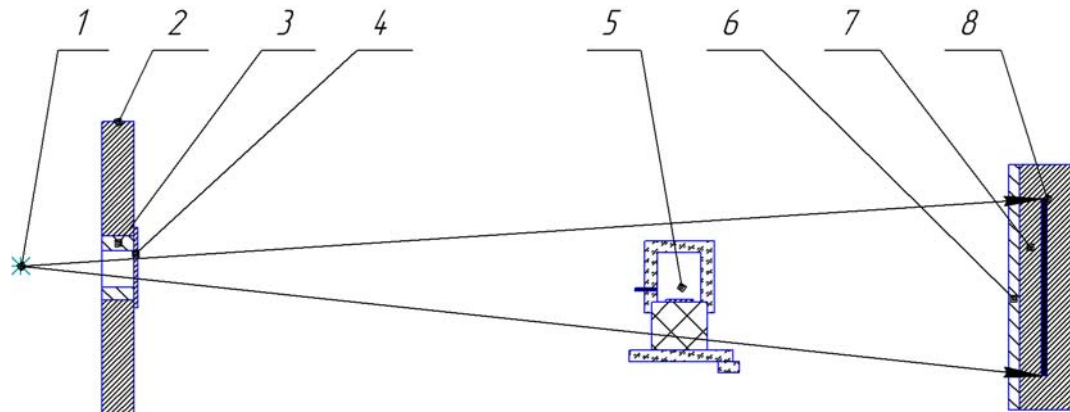
Numerical simulation of experiments was implemented with the use of Eulerian technique and Lagrangian technique. In accordance with the results of numerical simulation the authors performed verification of parameters of a relaxation model of beryllium strength.

The following RFNC-VNIIEF experts took part in the work: O.N. Aprelkov, N.L. Boriskova, V.V. Gorbunov, A.V. Zaytsev, D.N. Zamotaev, V.V. Igonin, O.N. Ignatova, D.V. Kryuchkov, A.I. Lebedev, M.O. Lebedeva, A.N. Malyshev, V.V. Markov, S.S. Nadezhin, V.A. Raevskiy, V.I. Skokov, A.N. Cheraev, V.V. Filyaev, M.A. Kaganov.

## 1 Used techniques

### 1.1 Radiographic technique

To investigate shear strength of *Be* when loading it up to pressures  $P \approx 10 \div 60$  GPa, the dynamic method of perturbations was used [3], [4]. The scheme of test conduction is presented in Fig.1.1.



- 1 – source of X-ray radiation;
- 2 – element of armor protection of bunker;
- 3 – collimator;
- 4 – protective screen;
- 5 – experimental assembly;
- 6 – protective screen;
- 7 – armored cassette;
- 8 – screens ADC – CR (10 units).

Fig. 1.1 – Scheme for conduction of tests

The facility «Eridan-3» was the source of X-ray radiation. Its boundary radiation energy is 1 MeV, pulse duration at a half-height is  $\sim 0.15 \mu\text{s}$ .

The information about the perturbation growth was obtained basing on X-ray image of the free surface of the liner under study. Recording of X-ray image was performed by using the one-frame regime at the package of photochromic screens ADC - CR [5]. The images, which were obtained in the screens, were summarized by special algorithm [5]. Mathematical processing of the images was performed by the package of programs [6], [7].

## 1.2 Laser-interferometric technique

The connection between perturbation growth and shear strength is determined basing on numerical simulation. In this case, it is very important to provide a reliable description of the loading regime of the liner, in particular, the  $P(t)$  dependence. The error of  $P(t)$  calculation can be caused by the inaccuracy of the equation of state of HE detonation products. The  $W(t)$  dependence of velocity on time is mostly determined by pressure of explosion products on a loaded surface and by the equation of state of beryllium. The numerical description of  $W(t)$  gives grounds to believe that  $P(t)$  is also calculated correctly.

To verify reliability of the  $P(t)$  calculation, measurements of the dependence of the velocity of beryllium liner free surface on time were performed in each X-ray test. The measurements were performed by a laser interferometer of the VISAR type [8].

A basic scheme of the experiment by using a laser interferometer for recording a rate of motion of a free surface is presented in Fig. 1.2.

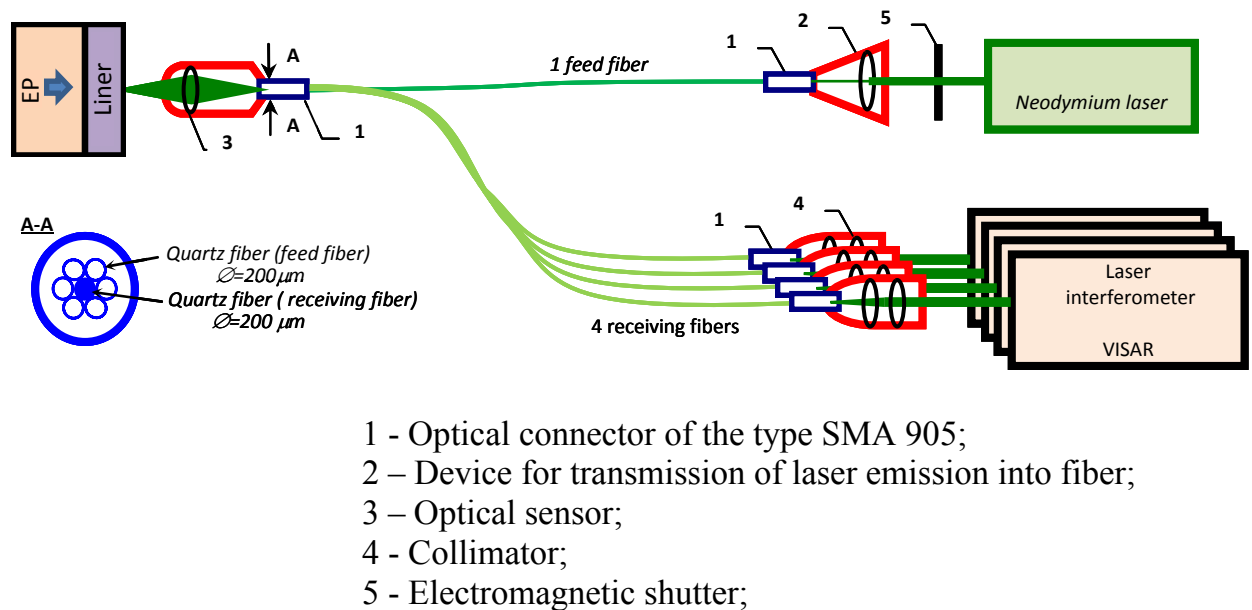


Fig. 1.2 - A basic diagram of the experiment by using a laser interferometer for recording a rate of motion of a free surface

To transfer laser emission, fiber-optic lines were used having a central core diameter of 200  $\mu\text{m}$ . In order to record a signal, four-channel oscillographs were used with a pass band of  $\sim 1$  GHz.

### **1.3 Manganin technique**

To record a pressure profile of SW, the technique of a manganin-based sensor (MS) was used, which was analogous to that described in work [9]. The results of its application for recording pressures in shock-wave processes were given, for example, in work [10]. The technique was made on the basis of a potentiometric measuring scheme with pulsed mode for supplying voltage towards a sensor.

To make measurements, foil gauges having four outputs were applied with rated resistance  $0.3 \, \Omega$  (Ohm) [10]. A sensing element of a gauge was made of foil with the thickness of  $30 \, \mu\text{m}$  and had sizes of  $0.5 \times 10 \, \text{mm}$  in a plan. A gauge was placed into insulating layers made of fluoroplastic; the total thickness of the gauge was  $0.23 \, \text{mm}$ . The gauge and the measuring scheme made it possible to record the pressure profile  $\sigma_x(t)$  with a rise front not more than 20 nanoseconds. Oscillographs with a frequency band of 300 MHz were used as a recorder.

The pressure was calculated according to the calibration dependence for foil manganin—based pressure sensors, which was specified by polynomial of the third power:

$$P = 36.91 \frac{\Delta R_d}{R_d} - 9.5385 \left( \frac{\Delta R_d}{R_d} \right)^2 + 20.421 \left( \frac{\Delta R_d}{R_d} \right)^3 + 0.224 \quad (1.3.1)$$

The error of determination  $\sigma_x$  accounted for not more than  $\pm 5 \, \%$  when using the calibration formula (1.3.1) defined in [10] for a range of pressures  $1 \div 45 \, \text{GPa}$ .

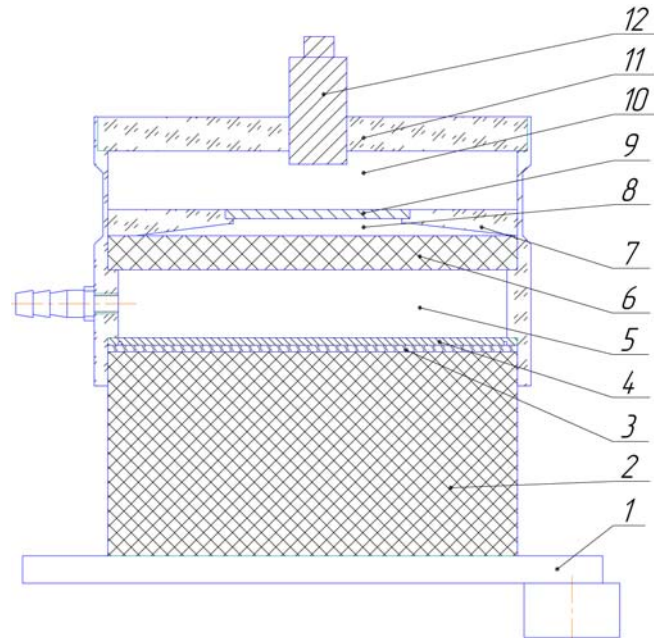


## 2 Experimental setup

### 2.1 Radiographic experiments

To investigate *Be* shear strength via the perturbation method in the pressure area up to  $P \approx 50$  GPa and at strain rates up to  $\dot{\epsilon} \sim 10^6 \text{s}^{-1}$ , the authors applied the experimental assembly, which was earlier used in work [11]. The scheme of the assembly is presented in Fig. 2.1.

A vacuumized gap of 2 mm between the investigated *Be* liner and HE cartridge of the second stage provided quasi-isentropic loading of a liner. HE with caloricity  $Q = 6.1$  KJ/g was used in the tests.



- 1 - generator of planar shock wave;
- 2 - HE of first stage:  $\varnothing 90 \times 80$  mm;
- 3 - damper: plexiglass,  $\varnothing 90 \times 2$  mm;
- 4 - impactor of first stage: *Fe*,  $\varnothing 90 \times 2.2$  mm;
- 5 - vacuumized gap:  $\delta = 10$  mm;
- 6 - HE of second stage:  $\varnothing 90 \times 10$  mm;
- 7 - bracket: Plexiglass;
- 8 - vacuumized gap:  $\delta = 2$  mm;
- 9 - studied liner: *Be*,  $\varnothing 50 \times 2$  (1.78) mm;
- 10 - vacuumized volume;
- 11 - disk: Plexiglass,  $\varnothing 90 \times 10$  mm;
- 12 - optical gauge.

Fig. 2.1 - Two-stage loading device for quasi-isentropic loading of *Be* liner.  $P \approx 50$  GPa

Fig. 2.2 presents the calculated dependences of loading pressure, velocity and displacement of a loaded surface of the investigated liner on time.

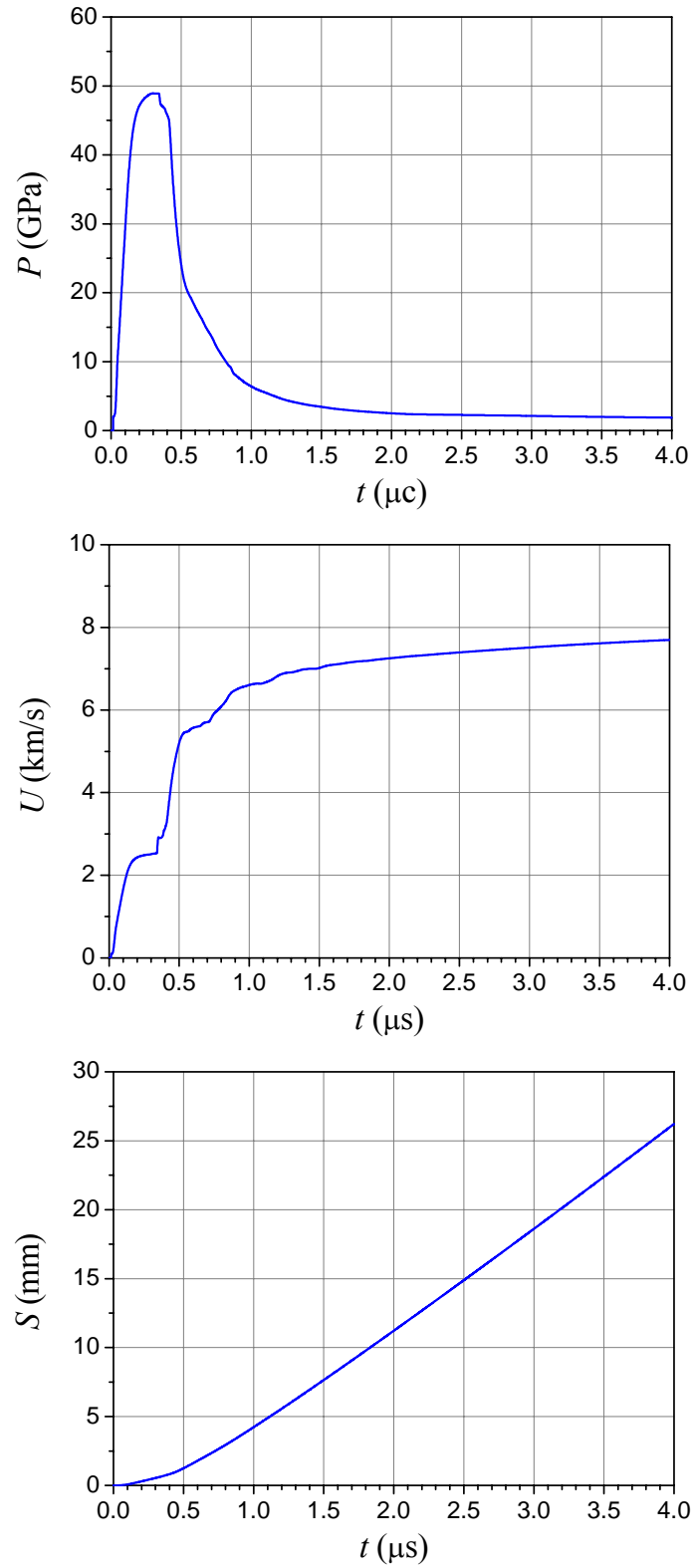


Fig. 2.2 - Time dependences of loading pressure, velocity and displacement of loaded surface of investigated *Be* liner under quasi-isentropic loading.  $P \approx 50$  GPa

According to estimations, when loading the liner, a strain rate was  $\dot{\epsilon}_i \sim 10^6 \text{ s}^{-1}$  in a compression wave. Increment of thermal energy was  $\Delta E_T \approx 416 \text{ J/g}$  after straining. Under normal conditions, thermal energy of *Be* was  $E_T \approx 547 \text{ J/g}$ . Thermal energy of *Be* was  $E_m \approx 2846 \text{ J/g}$  at the beginning of melting. Therefore, thermal energy of *Be* after deformation was  $\approx 34 \%$  of melting energy  $E_m$ . Increment of thermal energy regarding the energy required for heating from the initial state to melting was  $\frac{\Delta E_T}{E_m - E_T} \approx 0.18$ .

Configuration of the liners was selected basing on two-dimensional calculations. Liners with the thicknesses  $h=1.78 \text{ mm}$  and  $h=2.0 \text{ mm}$  were used in experiments. Configuration of the liner with the thickness  $h=2.0 \text{ mm}$  is presented in Fig. 2.3. A design of the liner with the thickness  $h=1.78 \text{ mm}$  was identical.

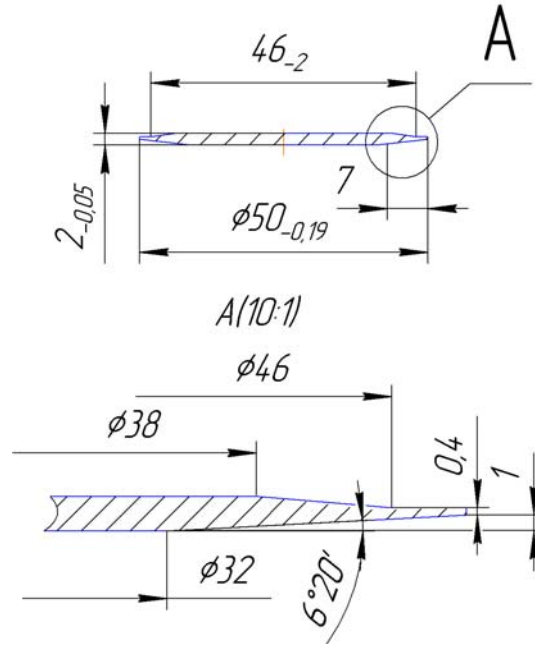


Fig. 2.3 – Configuration of liner with thickness  $h=2.0 \text{ mm}$

Periodic perturbations were specified at loaded surfaces of liners. The perturbations were extended sinusoidal recesses (grooves). The order of recesses determined the perturbation wave length  $\lambda$ , and a depth determined the initial amplitude  $A_0$  (amplitude  $A_0=2a_0$ ,  $a_0$  is a traditionally used designation of amplitude at a harmonically varied function). The order of recesses was  $\lambda=4 \text{ mm}$ . The amplitude of perturbations amounted to  $A_0 \approx 0.38 \text{ mm}$  for liners having a thickness  $h=1.78 \text{ mm}$ , it amounted to  $A_0 \approx 0.48 \text{ mm}$  for liners with the thickness  $h=2.0 \text{ mm}$ .

## **2.2 Experiments with recovery of samples**

The goal of these investigations was to determine how loading and SW strength influence on *Be* microstructure. Two types of loading can be used in the experiments:

- loading by a quasi-isentropic compression wave, which is transformed into a shock wave gradually (a maximum pressure is constant, a strain rate is changed from  $\dot{\epsilon}_x \sim 10^5$  to  $10^{10} \text{ s}^{-1}$ );
- loading by a thin metal impactor, which reduces amplitude of an entering shock wave a several times while moving in the sample (SW amplitude is changed  $P \sim 65 \div 30 \text{ GPa}$ , a strain rate is  $\dot{\epsilon}_x \sim 10^{10} \text{ s}^{-1}$ ).

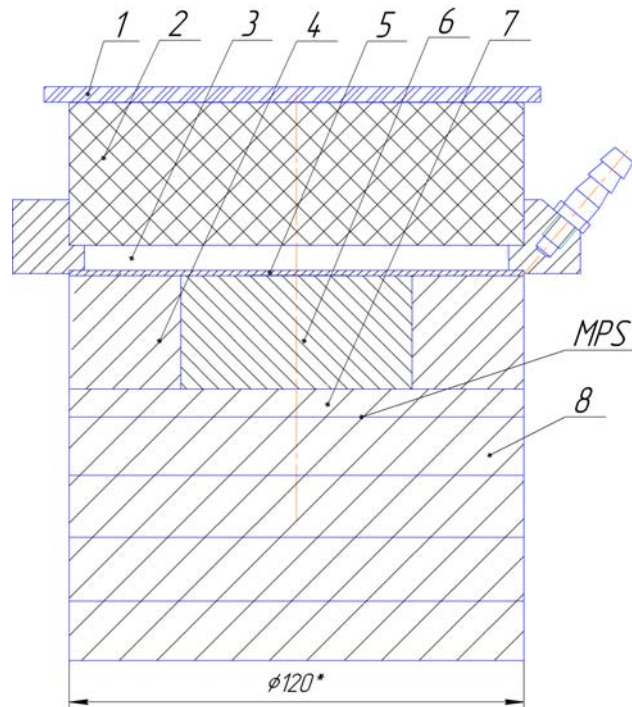
Experimental set-up was selected on the basis of numerical calculations in such a way that tensile stresses do not occur in beryllium samples after a main loading pulse, which could cause a fracture of samples. Beryllium samples under study were placed into the Al-cartridge of a great diameter. Aluminum was chosen due to the values of dynamic impedance most closely related to beryllium (the product of density by a sound speed). A beryllium sample was loaded via explosion products of HE through a gap in test №1 or by a thin aluminum impactor being accelerated by explosion products through a gap in test №2. The composition based on HMX was used as loading HE in both tests. Several aluminum discs were arranged at the exit from the cartridge for the purpose of absorbing a mechanical pulse. Deceleration and recovery of the beryllium sample under investigation were implemented for test №1 in a sand layer of the size  $0.6 \times 0.6 \times 0.6 \text{ m}$ , for test №2 - in a combination of concrete of the size  $0.6 \times 0.6 \times 0.3 \text{ m}$  with sand of the size  $0.6 \times 0.6 \times 0.3 \text{ m}$ .

To check a loading pressure, manganin-based pressure sensors were installed between aluminum disks. Sensitive elements of sensors *D1* and *D2* were located at the diameter of  $\sim 20 \text{ mm}$ . When installing sensors, epoxy adhesive was applied to remove air from a gap between disks.

Metallographic investigations of beryllium samples were performed after tests. Samples were being studied using an optical metallurgical microscope at magnifications of  $50^{\times}$ - $500^{\times}$ . Metallographic sections were photographed by using a digital photo camera. As a result of investigations, dislocation density of twins was determined.

### 2.2.1 Assembly №1. Transition of quasi-isentropic compression wave into SW

Fig. 2.4 presents a sketch of experimental assembly.



- 1 - generator of planar shock wave;
- 2 - HE:  $\phi 120 \times 30.7$  mm;
- 3 - vacuumized gap:  $\Delta = 3$  mm;
- 4 - cartridge: Al  $\phi 120 \times 15$  mm;
- 5 - disk: Al  $\phi 120 \times 0.5$  mm;
- 6 – recovered sample: Be  $\phi 60 \times 15$  mm<sup>4</sup>
- 7 - disk: Al  $\phi 120 \times 5$  mm;
- 8 - disk: Al  $\phi 120 \times 10$  mm - 4 pieces;
- MPS – manganin-based pressure sensors.

Fig. 2.4 – Sketch of experimental assembly №1

Fig. 2.5 presents the dependences of stress on time at various depths  $X$  of a beryllium sample (a counting from the loaded surface).

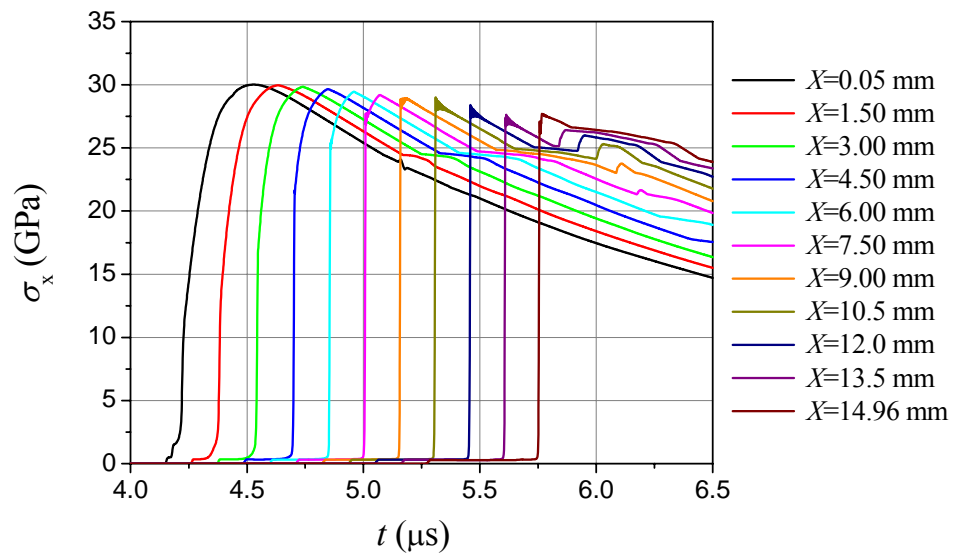


Fig. 2.5 – Stress versus time at various depths of beryllium sample

Fig. 2.6 demonstrates the dependencies of intensity of plastic strain on time at various depths of *Be* sample (the counting from the loaded surface).

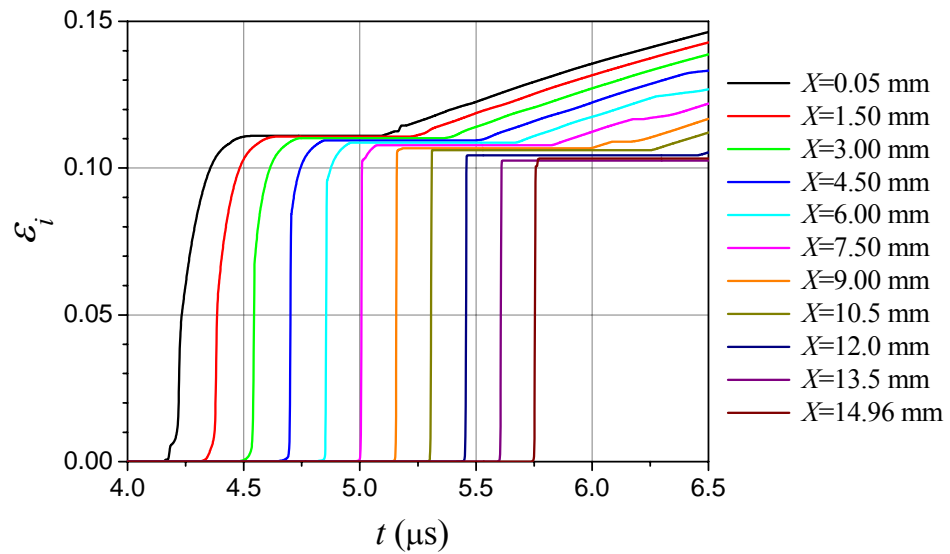


Fig. 2.6 – Intensity of plastic strain versus time at various depths of beryllium sample

Fig. 2.7 demonstrates the dependencies of yield strength on time at the various depths of a beryllium sample (the counting from the loaded surface).

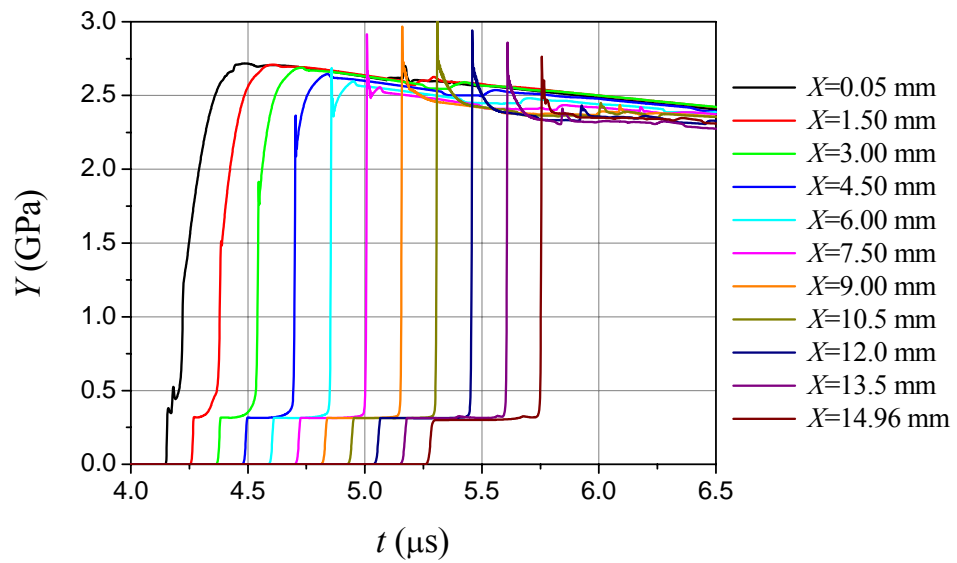


Fig. 2.7 – Yield strength versus time at various depths of beryllium sample

Fig. 2.8 presents the time dependence on the temperature on at the various depths of a beryllium sample (the counting from the loaded surface). The melting temperature lies in the range of  $1750 \div 2300$  °K at the same depths.

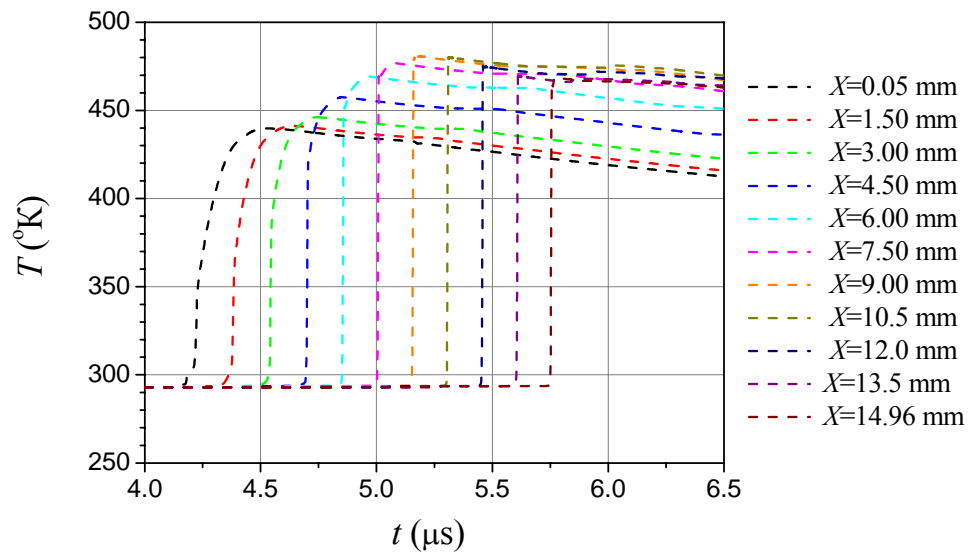
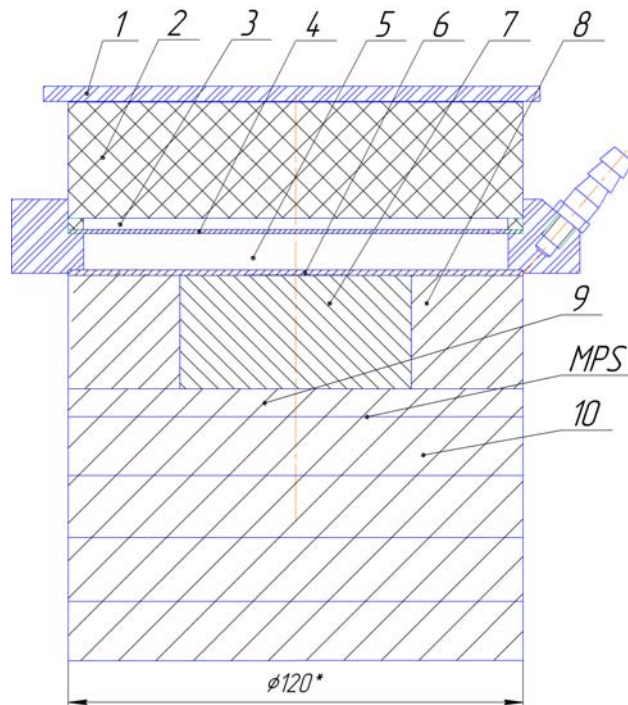


Fig. 2.8 – Time dependence on temperature at various depths of beryllium sample

### 2.2.2 Assembly 2. Shock wave loading of decreasing amplitude

Fig. 2.9 presents a sketch of experimental assembly.



- 1 - generator of planar shock wave;
- 2 - HE:  $\varnothing 120 \times 30.7$  mm;
- 3 - vacuumized gap:  $\Delta = 5$  mm;
- 4 - impactor: Al  $\varnothing 120 \times 2$  mm;
- 5 - vacuumized gap:  $\Delta = 10$  mm;
- 6 - disk: Al  $\varnothing 120 \times 2$  mm;
- 7 - recovered sample: Be  $\varnothing 60 \times 30$  mm;
- 8 - cartridge: Al  $\varnothing 120 \times 30$  mm;
- 9 - disk: Al  $\varnothing 120 \times 5$  mm;
- 10 - disk: Al  $\varnothing 120 \times 10$  mm - 4 pieces;
- MPS – manganin-based pressure sensors.

Fig. 2.9 – Sketch of experimental assembly №2

Fig. 2.10 presents the dependences of stress on time at the various depths of a beryllium sample (the counting from the loaded surface).



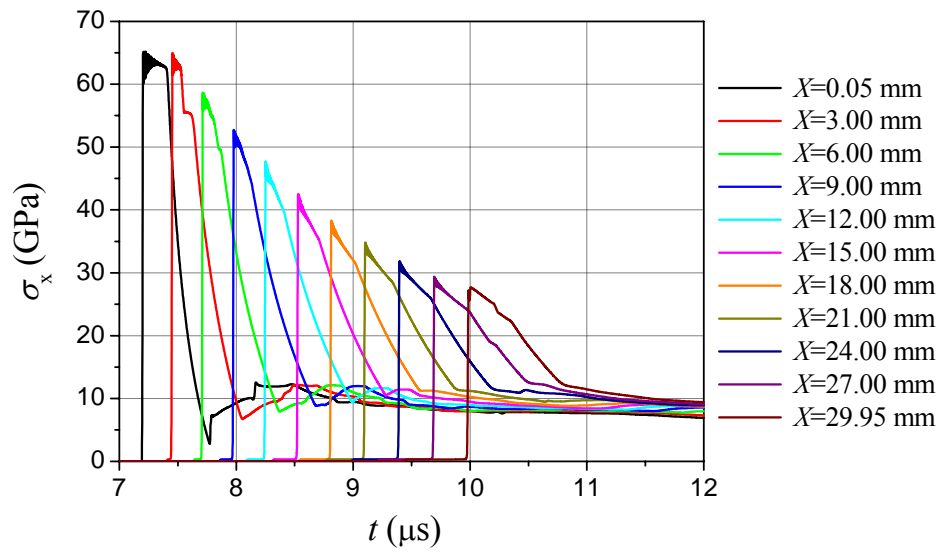


Fig. 2.10 – Dependencies of stress on time at various depths of beryllium sample

Fig. 2.11 presents the dependences of intensity of plastic strain on time at the various depths of a beryllium sample (the counting from the loaded surface).

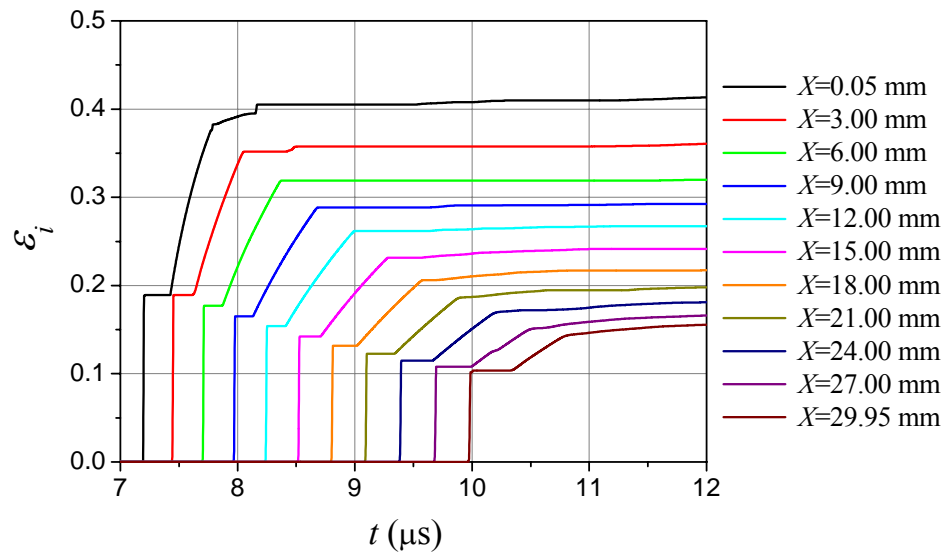


Fig. 2.11 – Dependencies of intensity of plastic strain on time at various depths of beryllium sample

Fig. 2.12 presents the dependences of yield strength on time at the various depths of a beryllium sample (the counting from the loaded surface).

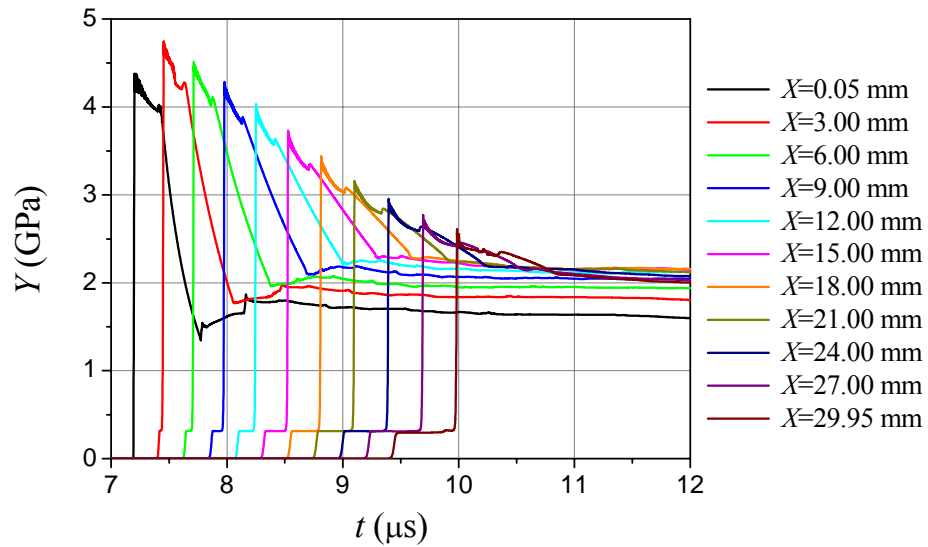


Fig. 2.12 – Dependencies of yield strength on time at various depths of beryllium sample

Fig. 2.13 presents the temperature dependence on time at the various depths of a beryllium sample (the counting from the loaded surface). The melting temperature is in the range of 1750÷2700 °K at the same depths of the sample.

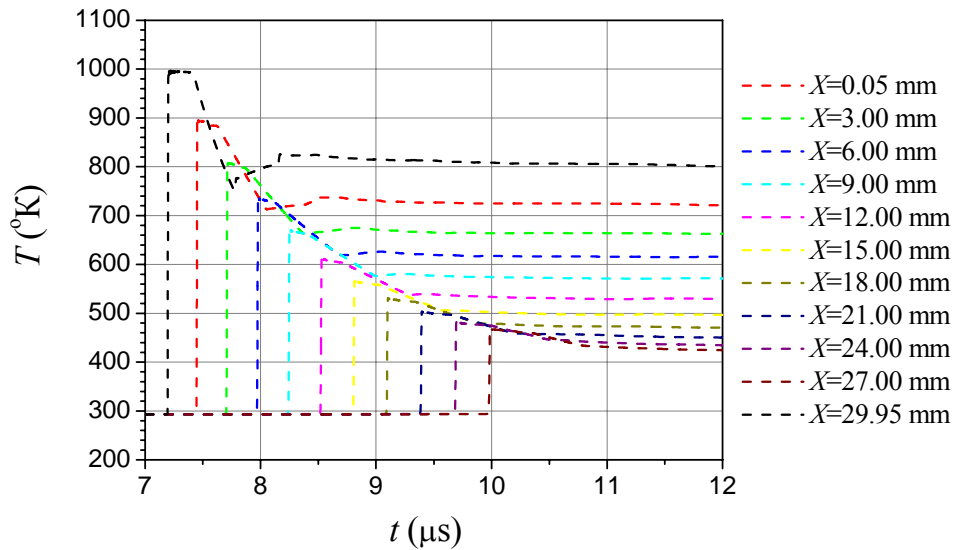


Fig. 2.13 – Temperature dependence on time at various depths of beryllium sample

### **3 Experimental results**

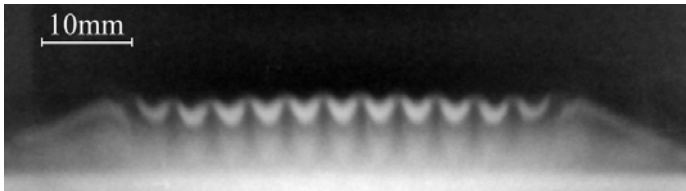
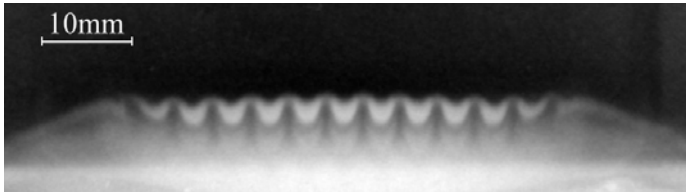
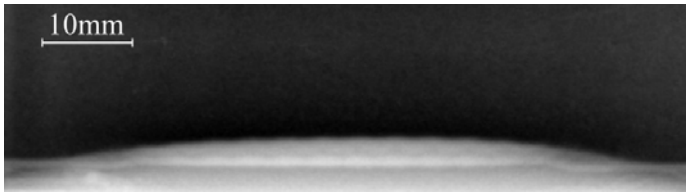
#### **3.1 Roentgenographic experiments**

The conditions of performance and the results of tests at quasi-isentropic loading of *Be* up to the pressure  $P \approx 50$  GPa are presented in Table 3.1. The following designations are used in Table 3.1:  $\lambda$  is the perturbation wavelength;  $A_0$  is the initial amplitude of perturbations (the amplitude is  $A_0 = 2a_0$ );  $h$  is the liner thickness,  $S$  is the distance travelled by the investigated liner by the time of recording;  $A$  is the amplitude (amplitude is  $A = 2a$ ) of perturbations by the time of recording.

It should be noted that the quality of X-ray image printing in paper does not allow one to show «fine» details, which can be seen in the monitor screen.

The time of the beginning of free surface motion accounted for  $48.8 \div 49$   $\mu\text{s}$  in five tests (see Chapter 3.2). This time amounted to  $48.8$   $\mu\text{s}$  for test №1 with the liner thickness  $h = 1.78$  mm. The authors planned to perform the second test with the liner thickness  $h = 1.78$  mm for the distance traveled by a plate at the time of X-ray radiography of  $4.5 \div 5$  mm. However, the assembly started with a slight delay and the time of the beginning of motion was  $49.35$   $\mu\text{s}$ . For this reason, the distance traveled by a plate at the moment of roentgenography was  $1.4$  mm in test №3.

Table 3.1 – Conditions of test conduction and experimental results. Quasi-isentropic loading, *Be*,  $P \approx 50$  GPa

Designation of test	$\lambda$ , mm	$A_0$ , mm	$h$ , mm	X-ray photo of investigated liner	$S$ , mm	$A$ , mm
Exp1	4	0.38	1.78		$8.9 \pm 0.3$	$2.7 \pm 0.2$
Exp2	4	0.48	2		$7.1 \pm 0.3$	$2.6 \pm 0.1$
Exp3	4	0.38	1.78		$1.4 \pm 0.2$	$0.6 \pm 0.1$

Continuation of Table 3.1

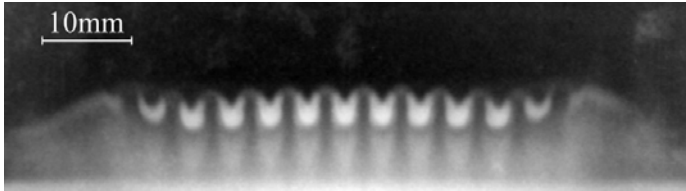
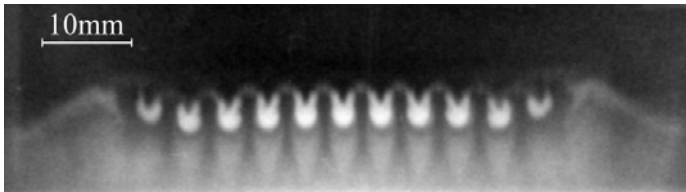
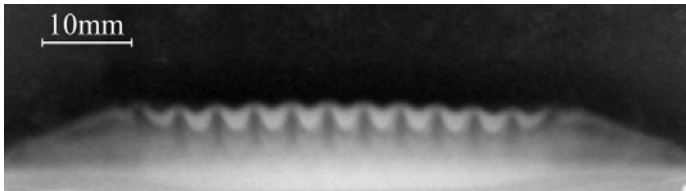
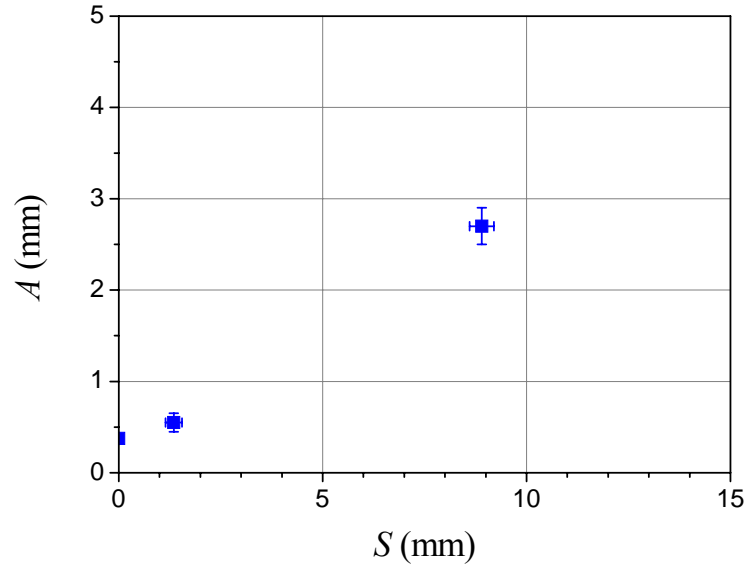
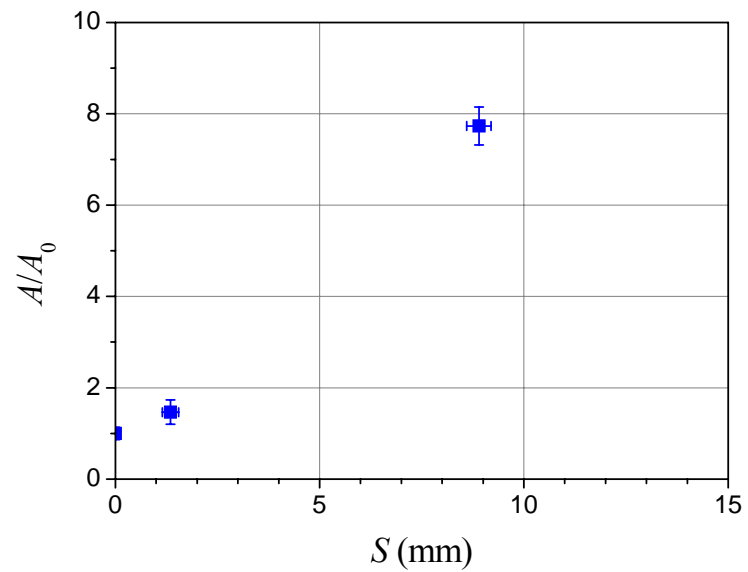
Designation of test	$\lambda$ , mm	$A_0$ , mm	$h$ , mm	X-ray photo of investigated liner	$S$ , mm	$A$ , mm
Exp4	4	0.48	2		$11.7 \pm 0.3$	$3.6 \pm 0.2$
Exp5	4	0.48	2		$14.6 \pm 0.5$	$4.1 \pm 0.2$
Exp6	4	0.48	2		$6.3 \pm 0.3$	$2.4 \pm 0.1$

Fig. 3.1 and Fig. 3.2 present the results of tests with the growth of periodic perturbations on a loaded beryllium surface under quasi-isentropic loading conditions up to the  $P_{\max} \approx 50$  GPa. The results are presented in absolute and relative units, respectively.

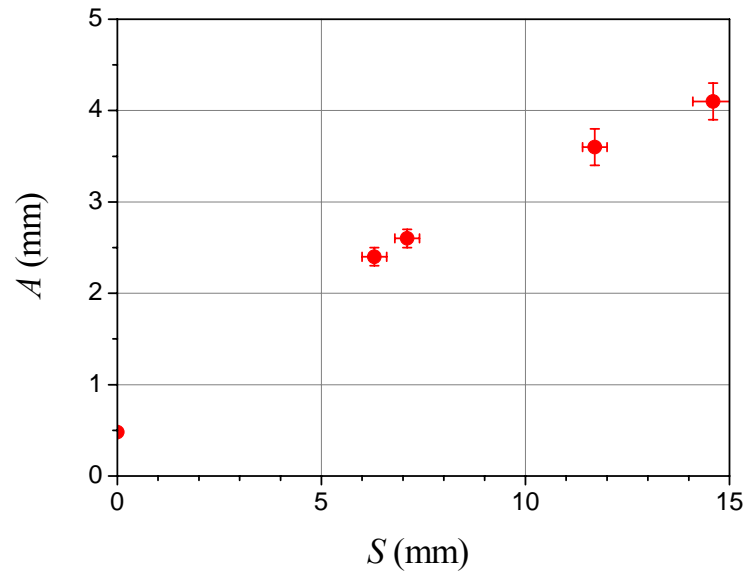


a)

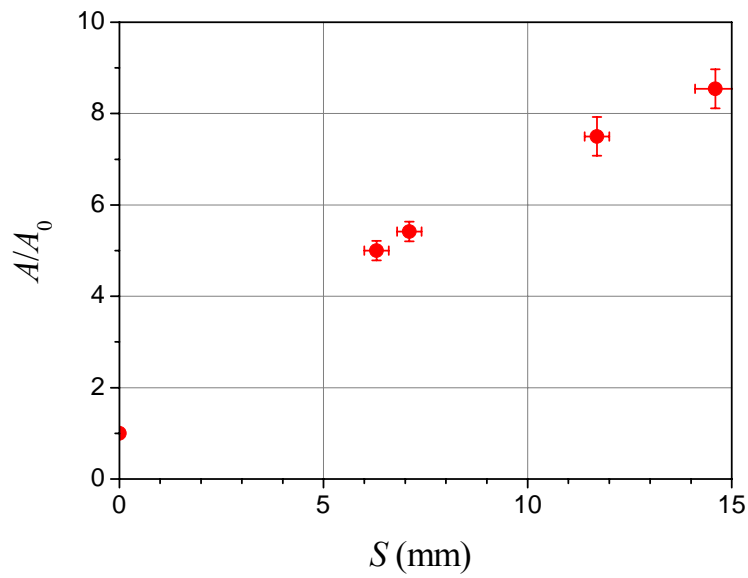


b)

Fig. 3.1 - Evolution of absolute (a) and relative (b) amplitudes of periodic perturbations  $A_0=0.38$  mm,  $\lambda=4$  mm,  $h=1.78$  mm, *Be*.  
Quasi-isentropic loading,  $P_{\max} \approx 50$  GPa



a)



b)

Fig. 3.2 - Evolution of absolute (a) and relative (b) amplitudes of periodic perturbations  $A_0=0.48$  mm,  $\lambda=4$  mm,  $h=2$  mm, *Be*.  
Quasi-isentropic loading,  $P_{\max} \approx 50$  GPa

### 3.2 Results of measurements via laser interferometer

The results of the measurements via a laser interferometer are presented in Fig. 3.3 - Fig. 3.8.

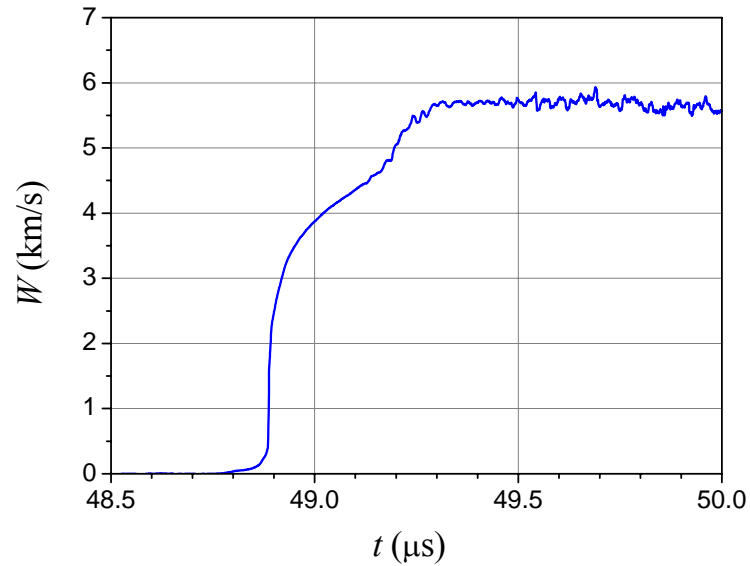


Fig. 3.3 - Results of measurements via laser interferometer. Test №1

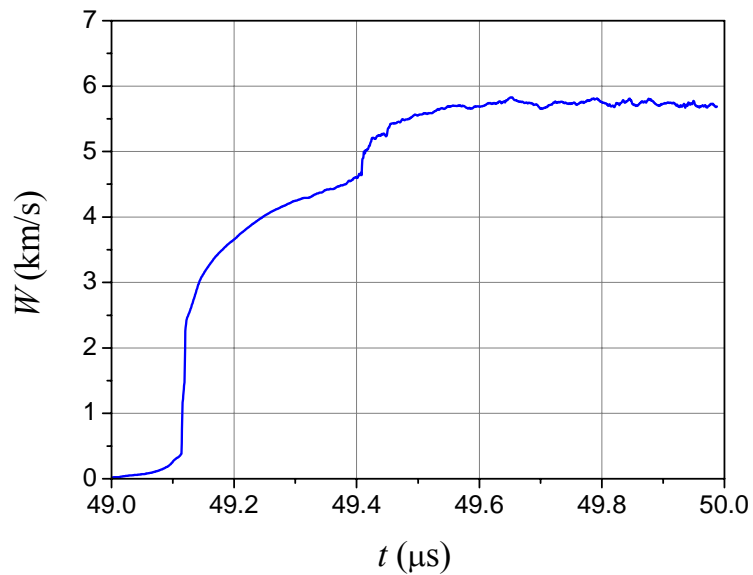


Fig. 3.4 - Results of measurements via laser interferometer. Test №2



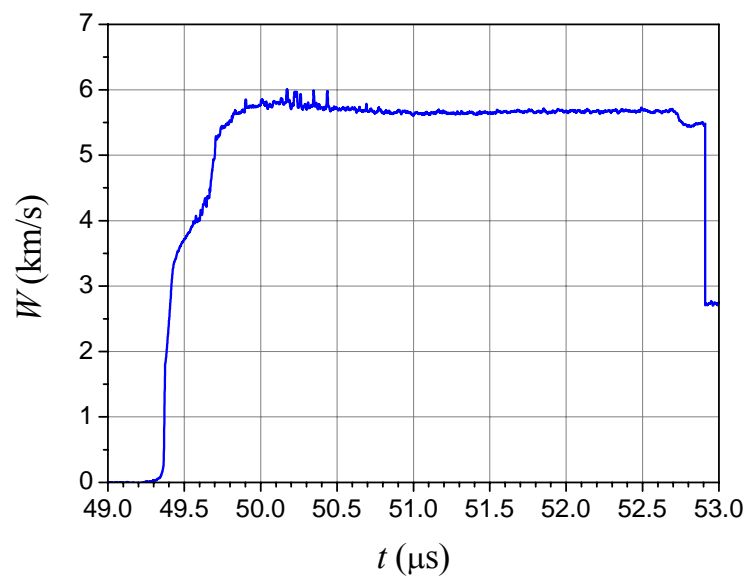


Fig. 3.5 - Results of measurements via laser interferometer. Test №3

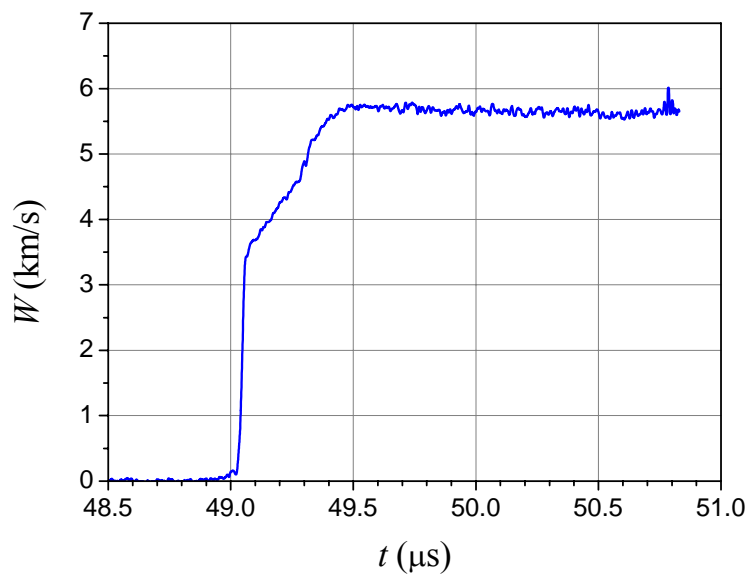


Fig. 3.6 - Results of measurements via laser interferometer. Test №4

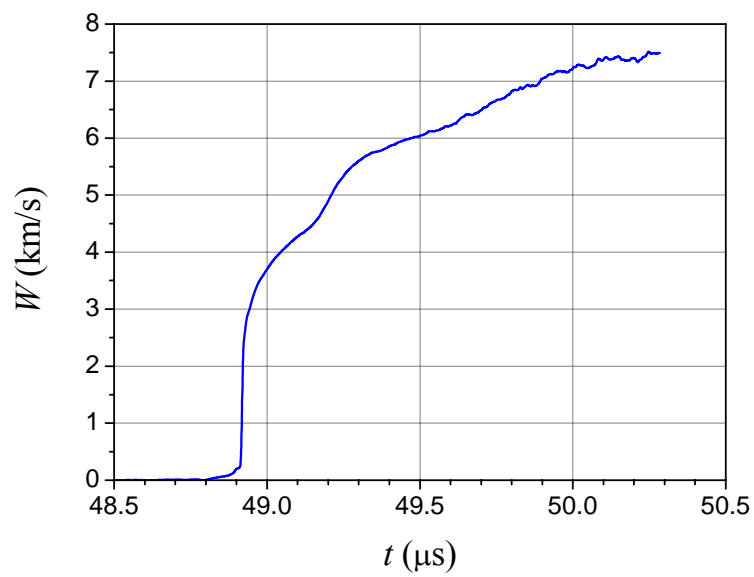


Fig. 3.7 - Results of measurements via laser interferometer. Test №5

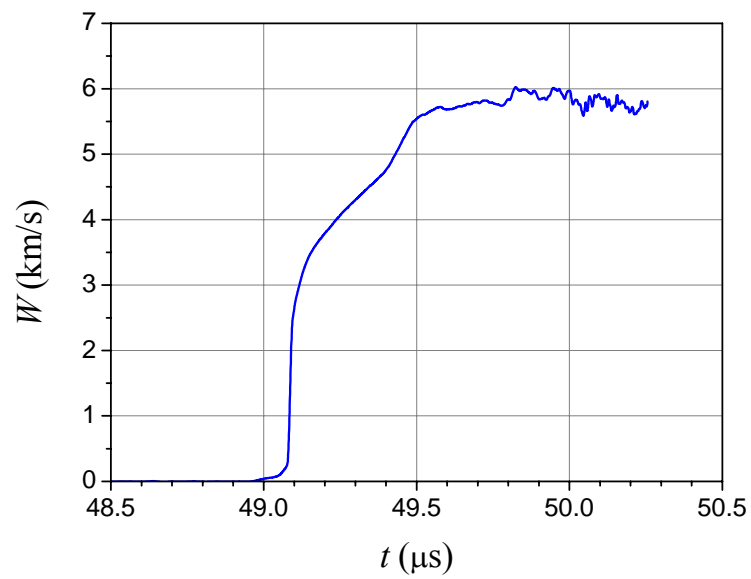


Fig. 3.8 - Results of measurements via laser interferometer. Test №6

It is obvious from the data presented in Fig. 3.3 - Fig. 3.8 that a free surface velocity was in the range of  $W \approx 5.7 \div 6$  km/s for five tests. In these tests the measurements were performed in the region of the maximum thickness of the liner, that is, an optical sensor of the laser was positioned into a center of a free surface - FS, under which there was a peak of perturbation. In test №5 with the maximum distance traveled by a plate at the moment of X-ray radiography  $S=14.6$  mm the measurements were implemented in the region of the minimum thickness of the liner, namely, the optical sensor of the laser was positioned into a center of a free surface - FS, under which a recess of perturbation occurred. As a result of loading, the material flowed from the initial recess towards the peak, then a recess was reduced in thickness from  $H=1.52$  mm to  $H=1.2$  mm and it was disrupted. A velocity of the thinnest liner part was  $W \approx 7.5$  km/s at the place of the initial recess.

### 3.3 Experiments with recovery of samples

#### 3.3.1 Test №1

As a result of loading in test №1, the aluminum cartridge and the beryllium sample were fractured. Sample's fragments found following the test are presented in Fig. 3.1.



Fig. 3.1 – Sample following test №1

Fig 3.2 presents the experimentally measured and calculated pressure profiles of manganin-based sensors *D1* and *D2*.

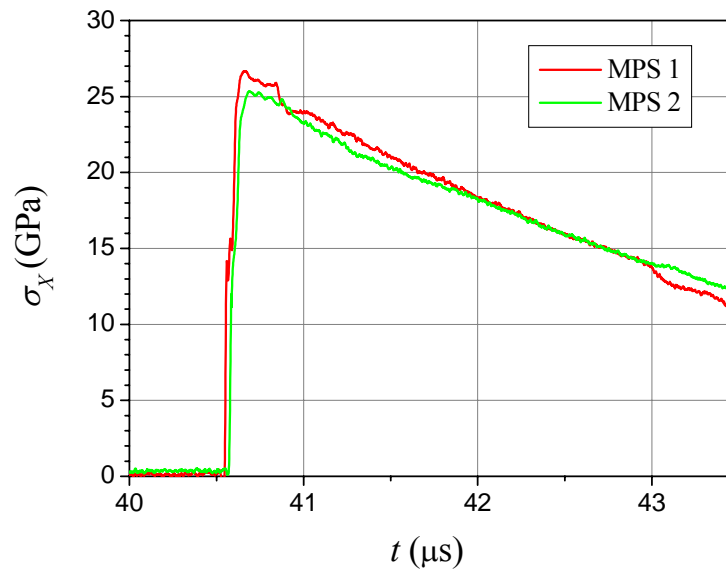


Fig 3.2 – Pressure profiles. Test №1

It is seen from Fig 3.2 that the amplitude of the shock wave issuing from the aluminum disk accounted for  $P_{sw} \approx 25$  GPa, diversity of operation of *D1* and *D2* sensors amounted to 0.02 μs.

### 3.3.2 Test №2

In test №2 the aluminum cartridge was damaged and the beryllium specimen was destructed partially. The photo of the sample is presented in Fig. 3.1.



Fig. 3.3 - Sample following test №2

Fig. 3.4 presents the experimentally measured and calculated pressure profiles of sensors *D1* and *D2*.

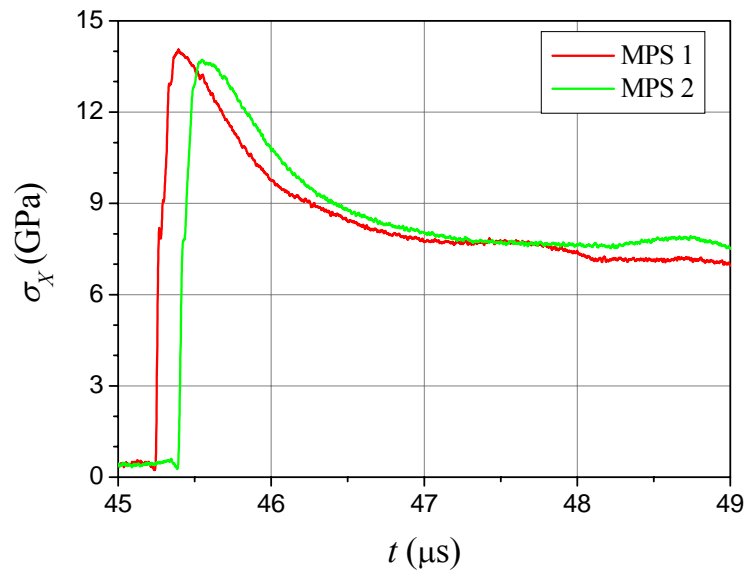


Fig. 3.4 – Pressure profiles. Test №2

It is seen from Fig. 3.4 that the experimentally measured amplitude of the shock wave leaving the aluminum disk accounted for  $P_{sw} \approx 14$  GPa. Diversity of operation of *D1* and *D2* sensors was 0.14 μs.

### **3.4 Results of metallographic investigations**

#### **3.4.1 Technique of metallographic analysis**

The technique of the metallographic analysis included the assessments of the nature and the extent of structural changes in the studied beryllium samples as a result of the action of dynamic loads on them.

The sample under investigation of test №2 was cut along the axis of symmetry, in the plane perpendicular to a shock front. A microsection was prepared for fine-structural investigations in the obtained section. For test №1 a microsection was prepared using a sample's fragment being remained after a test. Selected surfaces were subjected to grinding and polishing by using a mechanical means via a traditional technique.

The method of chemical etching was used to reveal a microstructure of the studied samples. Etching was performed when using a mixture of hydrofluoric acid and nitric acid with chrome anhydride at room temperature. The microstructure was revealed under chemical etching through immersion of microsection surface into an etchant.

The prepared microsections were investigated by optical metallographic microscope AXIOVERT 40 MAT at the magnifications of  $50^{\times}$ - $1000^{\times}$  in light background and in polarized light.

### **3.4.2 Test № 1**

The photo of the microsection of sample №1 is presented in Fig. 3.9.



Fig. 3.9 - Microsection of sample №1. General view

The photo of the microstructure of sample №1 is presented in Fig. 3.10. The sample has a fine-grained structure, average grain size in the sample is  $14.1 \pm 6.7 \mu\text{m}$  and a form of grains is close to an equiaxed form (Fig. 3.10).

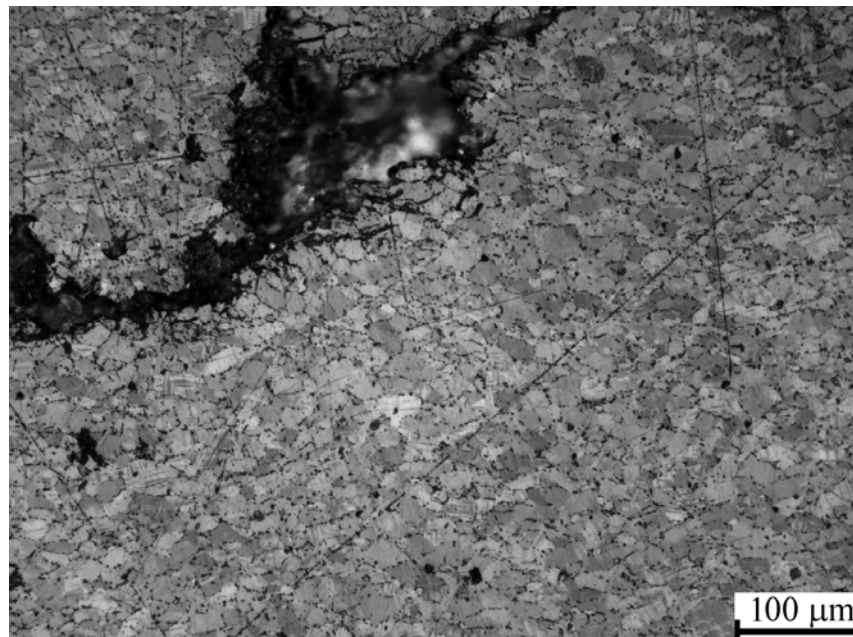


Fig. 3.10 - Photo of the microsection of sample №1



As a result of the shock action the sample was split in some places (Fig. 3.10). Bands of localized deformation are seen inside of grains, which can have twin origin. Bands of localized deformation within grains in sample №1 are presented in Fig. 3.11.

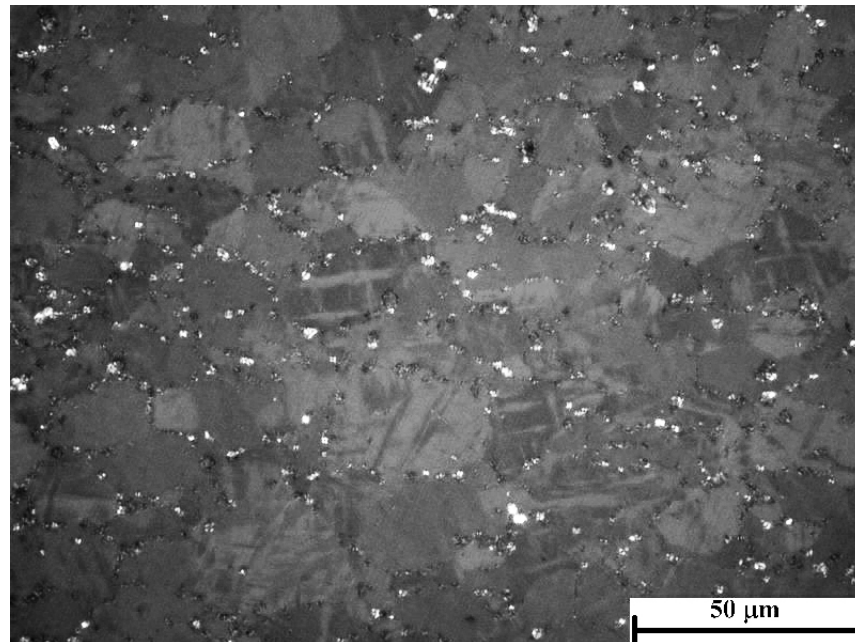


Fig. 3.11 - Bands of localized deformation within grains in sample №1.  
Photo in polarized light

The concentration of the grains containing such bands was not revealed in accordance with the distance from a loading surface, this concentration amounts to 37-47 % in the whole volume (it is identical in both samples).



### 3.4.3 Test № 2

Photo of the microsection of sample №2 is presented in Fig. 3.12.



Fig. 3.12 - Microsection of sample №2. General view

The sample was loaded in the direction from *B* to *H* (*B* is the sample's top, *H* is the sample's bottom). Sample №2 as well as sample №1 has a fine-grained equiaxed structure, in places with cracks (Fig. 3.13). The microstructure of sample №2 is presented in Fig. 3.13 - Fig. 3.14. The average measured grain size is  $14.4 \pm 7.3 \mu\text{m}$ . A structure of the sample is identical to sample №1.

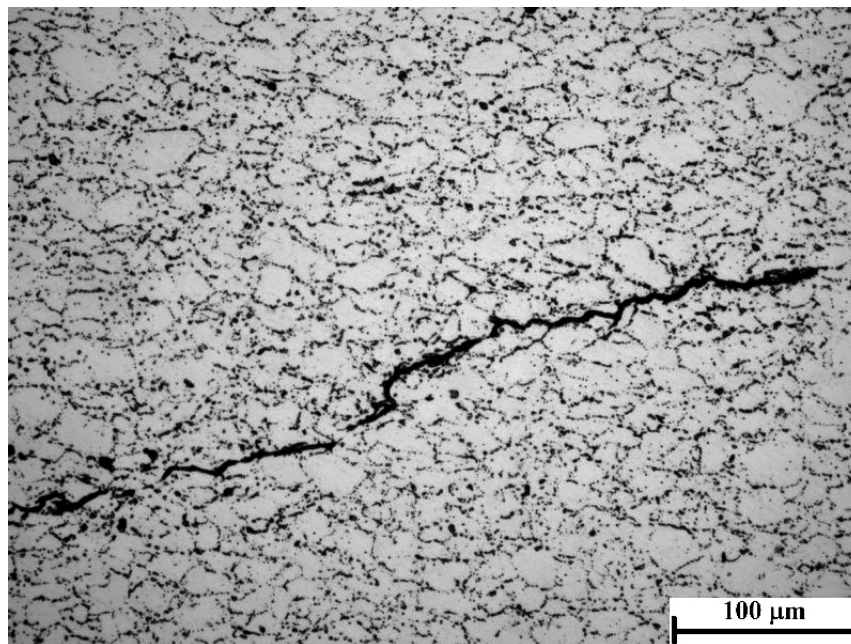


Fig. 3.13 - Microstructure of sample № 2

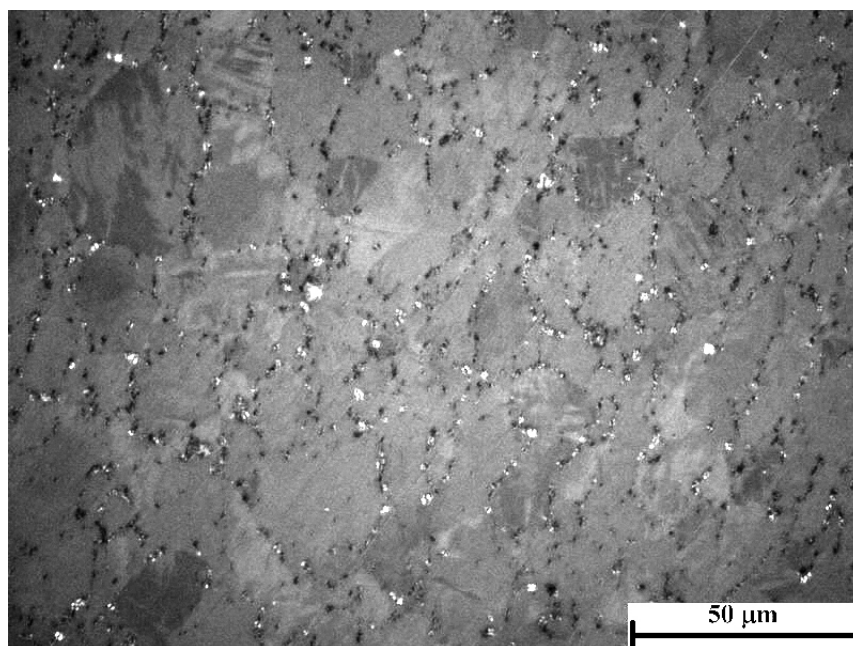


Fig. 3.14 - Photo of sample №2 in polarized light

#### **3.4.4 Discussion of results**

Unfortunately, we have no microstructure of a material prior to loading at our disposal; therefore, we can not arrive at the conclusions regarding a question what changes relate to its consequence (except for cracks). Obviously, it is necessary to search for traces of high-rate strain of beryllium at a more subtle level - by applying electron microscopy.

## 4 Relaxation model of beryllium strength (RING)

Below we present the model of beryllium shear strength, which is under development in VNIIEF, and which was used in calculations [12]. The model parameters were selected based on available experimental data. These data can be updated after obtaining the new experimental information.

### 4.1 Equations of state

In the area of pressures lower than 100 GPa, the spherical component of stress tensor can be presented in the simplified Mie-Grueneisen form with constant heat capacity:

$$\begin{aligned} P &= P_e(V) + \Gamma_p \cdot \rho \cdot C_v \cdot T \cdot D\left(\frac{\Theta}{T}\right), \\ E &= \frac{C_{0K}^2}{n} \left[ \frac{\delta^{n-1}}{n-1} + \frac{1}{\delta} - \frac{n}{n-1} \right] + E_T. \end{aligned} \quad (4.1)$$

In expression (4.1):  $\frac{\rho_{0K} C_{0K}^2}{n} (\delta^n - 1) = P_e$  is the elastic component of pressure,  $\rho_{0K}$ ,  $C_{0K}$  are the density and volume sound velocity at  $T=0$  °K,  $\Gamma_p$  is the Grueneisen coefficient,  $\rho$  is the substance density,  $\delta = \frac{\rho}{\rho_{0K}}$  is the relative compression,  $C_v = \frac{3R}{A}$  is the specific heat capacity at constant volume (the Dulong-Petit law);  $D\left(\frac{\Theta}{T}\right)$  is the Debye function,  $\Theta$  is the Debye temperature.

Because of a high value of the beryllium Debye temperature ( $\Theta=1031$  K), its specific heat  $C_v$  is much lower than the value  $\frac{3R}{A}$  at the normal temperature, and it is a function of the current temperature. Respectively, specific heat energy is less than the value  $\frac{3R}{A} \cdot T$ , and it can be written as follows:  $E_T = E_{T0} + \int_{T_0}^T C_v(T) dT$ , where  $E_{T0} = \int_0^{T_0} C_v(T) dT$  is the specific heat energy at normal temperatures. Calculations give the value  $E_{T0}=183$  J/g.

The equations of state are based on the available data on the measurement of the  $D$ - $U$  diagrams of compression [13], a sound velocity behind shock wave front [14], etc. [15]. The Grueneisen coefficient  $\Gamma_P$  is assumed as a function of only density (or relative compression ( $\delta$ )) [16]. It is true for not too high temperatures.

$$\Gamma_P = \Gamma_\infty + \frac{\Gamma_0 - \Gamma_\infty}{\delta^M}, \quad (4.2)$$

where  $\Gamma_0$ ,  $\Gamma_\infty$  are the values of  $\Gamma_P$  at  $\rho=\rho_{0K}$  and  $\delta \rightarrow \infty$  respectively.

The beryllium Grueneisen coefficient  $\Gamma_P$  is  $\Gamma_0=1.15$ ,  $\rho_{0K}=1.86 \text{ g/cm}^3$  under the normal conditions according to [17]. According to [18]  $\Gamma_0=1.17$ , and at  $\delta=1.66$   $\Gamma_P=1.0$ . In accordance with the calculations by using formula (4.2) with parameters from Table 4.1 the beryllium Grueneisen coefficient is equal to  $\Gamma_P=0.96$  at  $\delta=1.66$ .

Table 4.1 presents constant coefficients of equations (4.1) and (4.2) for beryllium. Parameters of the physical equation were selected to meet the conditions:  $P=0$  at  $\rho = \rho_0$ ,  $T=273 \text{ }^\circ\text{K}$  and  $P=0$  at  $\rho = \rho_{m0}^*$ ,  $T=T_{m0}=1557 \text{ }^\circ\text{K}$ .

Table 4.1 - Constant coefficients of beryllium equations (4.1) and (4.2) of beryllium

$\rho_{0K}$ (g/cm <sup>3</sup> )	$\rho_0$ , (g/cm <sup>3</sup> )	$C_{0K}$ , (m/s)	$n$	$\Gamma_\infty$	$\Gamma_0$	$M$	$C_V^{**}$ , (J/gK)
1.8668	1.85	8.03	2.89	0.5	1.25	1.0	2.7

\*  $\rho_{m0}$  is the melting density at  $T=T_{m0}$ ,  $T_{m0}$  is the melting temperature under the normal conditions ( $P=0$ ,  $\delta_{m0}=0.9145$ ).

\*\*  $C_V=2.7 \text{ J/gK}$  should be assumed at  $T>1031 \text{ }^\circ\text{K}$ . At  $T=293 \text{ }^\circ\text{K}$   $C_V=1.627 \text{ J/gK}$ .

## 4.2 Shear modulus and melting temperature

Shear modulus, which determines the deviator component of stress tensor in the elastic area of strain, is usually calculated by the formula:

$$G = \frac{3}{2} \cdot \frac{1-2\nu}{1+\nu} \cdot \rho \cdot C_B^2, \quad C_B^2 = \left( \frac{\partial P}{\partial \rho} \right)_s, \quad (4.3)$$

where  $\nu$  is the Poisson's ratio;  $C_K$  is the current volume sound velocity.

The dependence of the Poisson's ratio  $\nu$  can be assumed as a function of temperature  $\nu(T/T_m)$ . And it can be presented in the following way:

$$\nu = \nu_0 \cdot \left( 1 + C \cdot \left( \frac{T}{T_m} \right)^K \right), \quad \bar{T} < 1 \quad (4.4)$$

$$\nu = 0.5, \quad T \geq 1,$$

where  $\bar{T} = \frac{T}{T_m}$ ,  $T$  is the current temperature,  $T_m$  is the melting temperature,  $\nu_0$ ,  $C$ ,  $K = \text{const.}$

At the shock wave front, the Poisson's ratio can be determined using the relation of the elastic sound velocity  $C_L$  and the volume sound velocity  $C_K$ :

$$\nu = \frac{3C_B^2 - C_L^2}{3C_B^2 + C_L^2} \quad (4.5)$$

Table 4.2 presents parameters for the dependence of the Poisson's ratio on the temperature in form (4.4).

Table 4.2 – Parameters of equation (4.4)

$\nu_0$	$C$	$K$
0.03	15.63	3.0

Formula (4.4) describes the reference value  $\nu = \nu_0 = 0.03$  at  $T = 300^\circ K$ , and  $\nu = 0.5$  at  $T = T_m$  that corresponds to the liquid state. To obtain the more justified dependence  $\nu = f(\rho, \bar{T})$ , it is required to have additional experimental data. When obtaining the additional experimental information, it is possible to revise the dependence  $\nu = f(\rho, \bar{T})$ . Fig. 4.1 shows calculated and experimental data [14], [19] on elastic  $C_L$  and plastic  $C_B$  sound velocities behind the shock wave front.

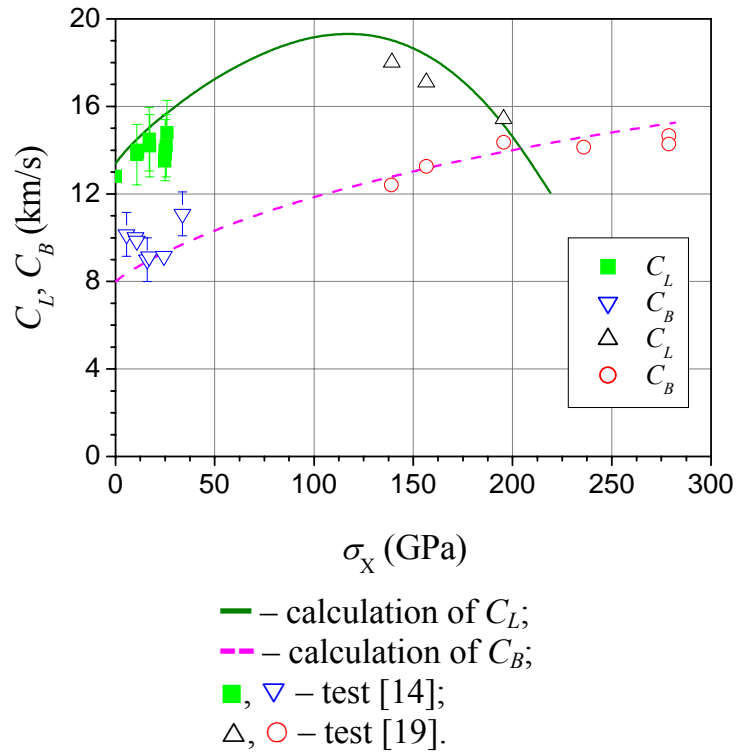


Fig. 4.1 - Calculated and experimental dependences of elastic  $C_L$  and plastic  $C_B$  sound velocities on pressure behind shock wave front

In the specified stress-strain state, the melting temperature  $T_m$  is determined by the Lindemann's law:

$$\frac{d \ln T_m}{d \ln \rho_m} = 2 \left( \Gamma_p - \frac{1}{3} \right),$$

where  $T_m$  is the melting temperature at density  $\rho_m$ .

At the initial conditions  $T_m = T_{m0}$ ,  $\rho_m = \rho_{m0}$ , the melting curve equation in the  $(\delta, T)$  plane has the form:

$$T_m = T_{m0} \left( \frac{\delta_m}{\delta_{m0}} \right)^{2 \left( \Gamma_\infty - \frac{1}{3} \right)} \exp \left[ \frac{2(\Gamma_0 - \Gamma_\infty)}{M} \left( \frac{1}{(\delta_{m0})^M} - \frac{1}{(\delta_m)^M} \right) \right], \quad (4.6)$$

where  $\delta_m = \frac{\rho_m}{\rho_{0K}}$ ,  $\delta_{m0} = \frac{\rho_{m0}}{\rho_{0K}}$  is the relative density of substance at  $T_m = T_{m0}$ , (the melting of the beginning),  $T_{m0}$  is the melting temperature in the normal state at  $P \approx 0$ . For beryllium,  $T_{m0} = 1557$  °K,  $\delta_{m0} = 0.9145$ .

Fig. 4.2 shows calculated and available experimental dependences of a temperature and a melting temperature.

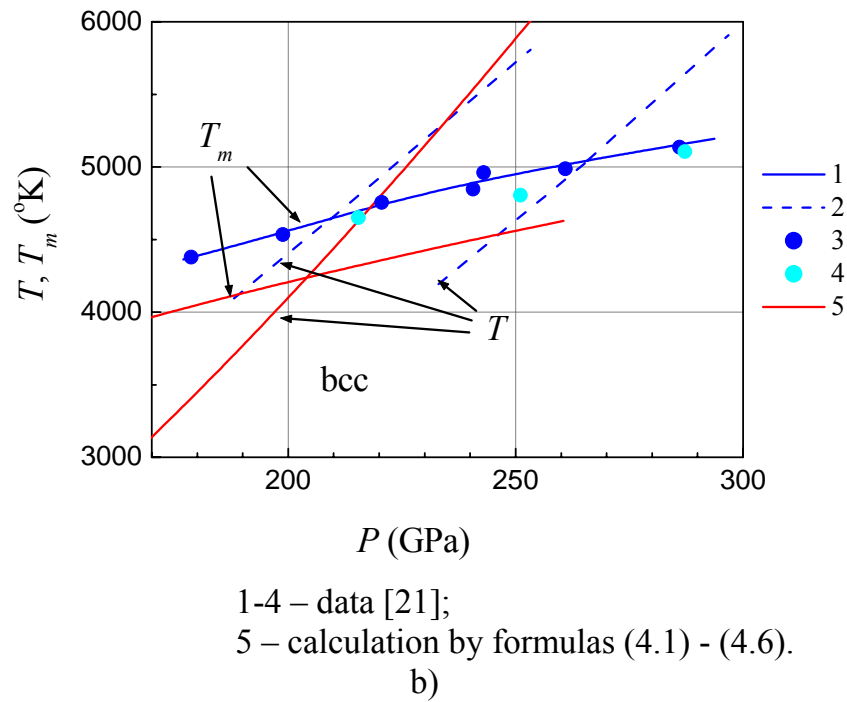
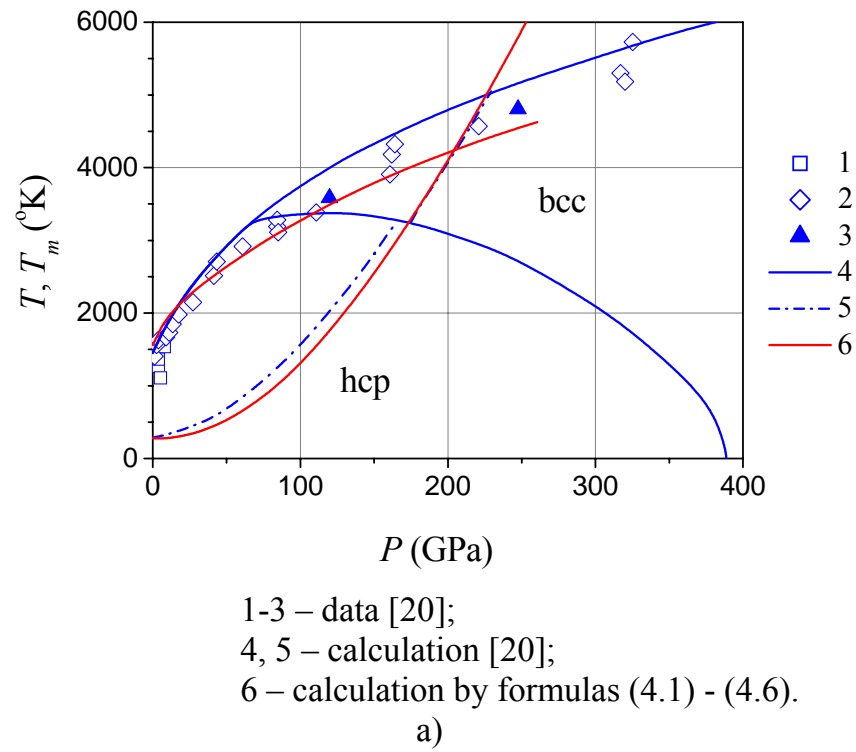


Fig. 4.2 – Experimental and calculated dependences of temperature and melting temperature along shock adiabat of beryllium



### 4.3 Relaxation model RING-I

For the more complete description of metal behavior at high-speed deformation, including shock-wave deformation, relaxation models of an elastic-plastic body are used. In these models, it is expected that the stress deviator depends on deviators of deformations and strain rates [22].

VNIIEF experts are using a simplified relaxation model, which involves usual elastic-plastic approximation, and dynamic yield strength is determined by a differential equation, which takes account of the process of relaxation of elastic stress. The basic equation, which determines the effective yield strength in the relaxing medium, is the following:

$$\dot{Y}_d = 3G\dot{\varepsilon}_i - \frac{Y_d - Y_s}{\tau}, \quad (4.7)$$

where  $Y_d$  is the effective yield strength at the present time,  $Y_s$  is the stationary yield strength, which occurs in a present state  $(P, T)$  of a substance at  $\dot{\varepsilon}_i=0$ ;  $\dot{\varepsilon}_i$  is the strain rate,  $\tau$  is the relaxation time for elastic stress. The points above  $Y_d$  and  $\varepsilon_i$  mean the derivative in time. As yield strength ( $\dot{Y}_d \cdot \tau \ll Y_d$ ) changes rather slow, equation (4.7) turns into an elastic-viscous-plastic model.

The stationary yield strength is presented in the following analytical form:

$$Y_s = Y_0 \cdot \left[ 1 + (a_1 \cdot (1 - \bar{T}^{a_3})) \cdot \left( 1 - \exp \left( -a_2 \cdot \left( \int_0^t \varphi_1(\dot{\varepsilon}_i) \cdot \dot{\varepsilon}_i dt \right) \right) \right) \right] \cdot \frac{G}{G_0}$$

$$\varphi_1 = \frac{1 + \varphi_{\max 1} \cdot \left( \frac{\dot{\varepsilon}_i}{\dot{\varepsilon}_{1s}} \right)^{a_4}}{1 + \left( \frac{\dot{\varepsilon}_i}{\dot{\varepsilon}_{1s}} \right)^{a_4}} \quad (4.8)$$

In equation (4.8)  $Y_0$ ,  $a_1$ - $a_4$ ,  $\varphi_{\max 1}$ ,  $\dot{\varepsilon}_{1s}$  are constant coefficients,  $G$ ,  $G_0$  is the shear modulus in the current state and the initial state respectively ( $G_0=160$  GPa). This equation takes account of the loading history, i.e. the dependence of hardening on strain rate and a value of strain [23]. Table 4.3 presents the parameters of equation (4.8).

Table 4.3 – Parameters of stationary yield strength of beryllium

$Y_0$ (GPa)	$a_1$	$a_2$	$a_3$	$a_4$	$\varphi_{max1}$	$\dot{\epsilon}_{1s}$ (s <sup>-1</sup> )
0.36	3.3	7.0	1.0	1.0	2.0	2.0

For relaxation time, the equation is used, which describes the tests on the measurement of a strain rate [24], [25] in shock wave front, compression diagrams and Taylor cylinders at  $\dot{\epsilon}_i < 10^5$  s<sup>-1</sup>:

$$\tau = \frac{\tau_0 \cdot (1 - \bar{T})^2}{\frac{G}{G_0} \cdot \left( 1 + \frac{\dot{\epsilon}_i}{\dot{\epsilon}_{i0}} \cdot \varphi_2(\dot{\epsilon}_i) \right)^{0.5}}, \text{ where} \quad (4.9)$$

$$\varphi_2(\dot{\epsilon}_i) = \frac{1 + \varphi_{max2} \cdot \left( \frac{\dot{\epsilon}_i}{\dot{\epsilon}_{2s}} \right)^{n_2}}{1 + \left( \frac{\dot{\epsilon}_i}{\dot{\epsilon}_{2s}} \right)^{n_2}}. \quad (4.10)$$

Equation (4.9) has the following limiting values:

at  $\dot{\epsilon}_i \rightarrow 0$ ,  $G = G_0$ ,  $\tau = \tau_0$ , at  $\bar{T} \rightarrow 1$  and (or)  $\dot{\epsilon}_i \rightarrow \infty$   $\tau \rightarrow 0$ .

With the parameters  $\varphi_{max2} = 156$ ;  $n_2 = 1.0$ ,  $\dot{\epsilon}_{2s} = 2 \cdot 10^3$  s<sup>-1</sup>,  $\tau_0 = 5$   $\mu$ s and  $\dot{\epsilon}_{i0} = 1$  s<sup>-1</sup> dependence in form (4.9) is in rather good agreement with experimental data up to strain rate  $\dot{\epsilon}_i \sim 10^8$  s<sup>-1</sup>.

In work [26] the results are presented for the description of the available experimental data through the model.

## 5 Results of numerical simulation of experiments with use of Eulerian technique

The authors made all calculations for the study of the perturbations growth on a loaded surface by using a two-dimensional gas-dynamic program on an immovable Eulerian grid in a plane geometry with the parameters of the equation of state of Mie-Grueneisen for beryllium taken from work [27].

Fig. 5.1 and Fig. 5.2 present the experimental results and the results of numerical simulation for the study of beryllium shear strength through «the method of perturbations» with the RING model.

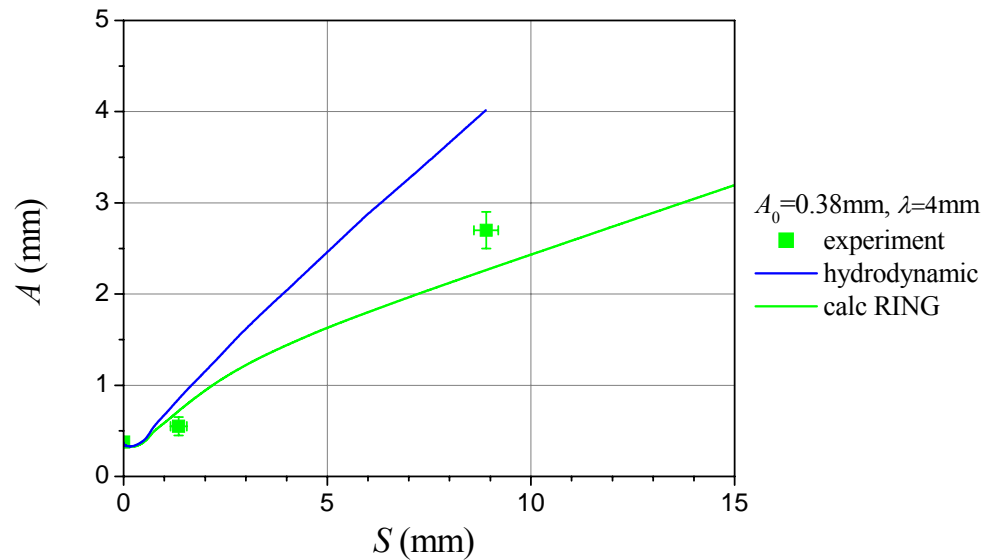


Fig. 5.1 – Experimental results and calculated dependencies of perturbation amplitudes on distance travelled by beryllium liner. Liner thickness  $\Delta = 1.78 \text{ mm}$

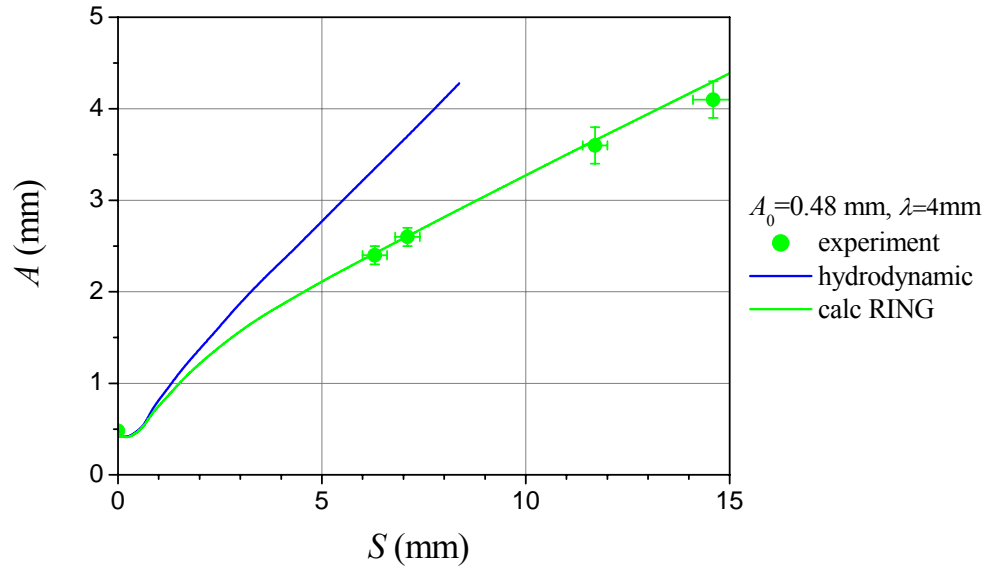


Fig. 5.2 - Experimental results and calculated dependencies of perturbation amplitudes on distance travelled by beryllium liner. Liner thickness  $\Delta=2.0$  mm

By analyzing Fig. 5.1 and Fig. 5.2, it may be concluded that the authors can make the conclusion that a growth of perturbations having initial amplitude  $A_0=0.48$  mm with the sample's thickness  $h=2$  mm is described adequately in the calculations with the dynamic strength model RING. In this case, both for the thickness of the sample  $h=1.78$  mm and for the initial amplitude  $A_0=0.375$  mm, there is only one experimental point in fact for the distance travelled by a plate at the time of X-ray radiography  $S \approx 8.9$  mm, which is not described via the dynamic strength model called RING.

Note that numerical description of the results of the majority of tests is satisfactory by using the RING models due to the fact that the initial amplitude of perturbations was great enough ( $A_0 \approx 0.48$  mm). In case of such great amplitude, the liner surface is in the conditions closely related to a hydrodynamical flow in a process of acceleration and the influence of strength is not considerable. It would be very useful to conduct analogous tests with the lower initial amplitude of perturbations, which is closely related to a stability threshold. In this regime the perturbation growth is more sensitive to shear strength and a checking of a strength model would be more reliable in such experiments.

In all the radiographic experiments the authors measured a dependence of a free surface velocity of a beryllium liner on time  $W(t)$  by the help of a laser-interferometric technique.

Fig. 5.3 - Fig. 5.8 present experimental and calculated dependencies of a free surface velocity (FS) of liners  $W(t)$ .

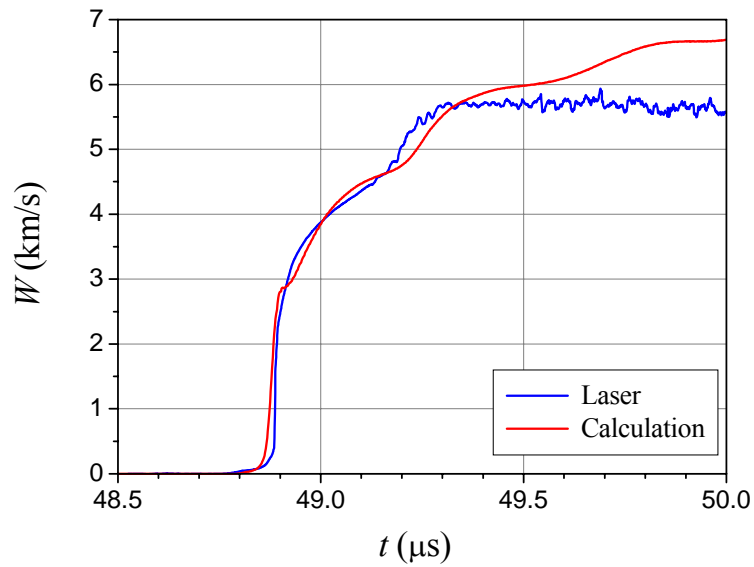


Fig. 5.3 - Experimental and calculated dependencies of free surface velocity on time  $W(t)$ .  
Liner thickness  $\Delta=1.78$  mm. Test №1

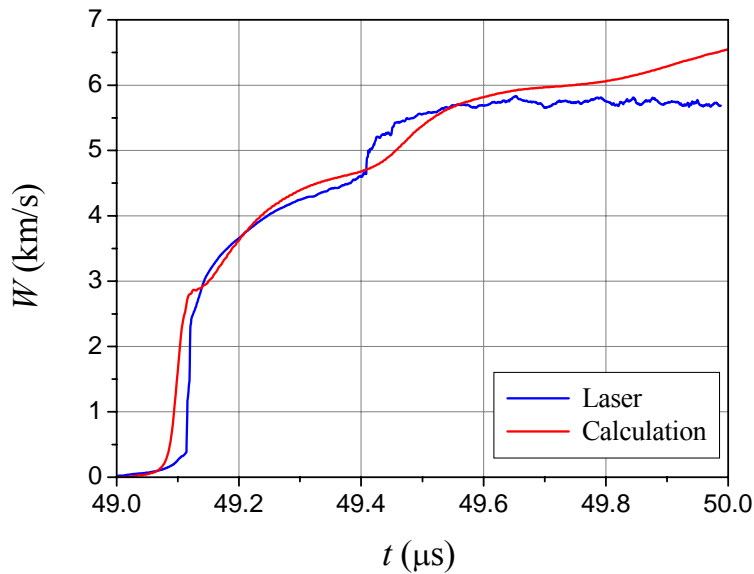


Fig. 5.4 - Experimental and calculated dependencies of free surface velocity on time  $W(t)$ .  
Liner thickness  $\Delta=1.78$  mm. Test №2

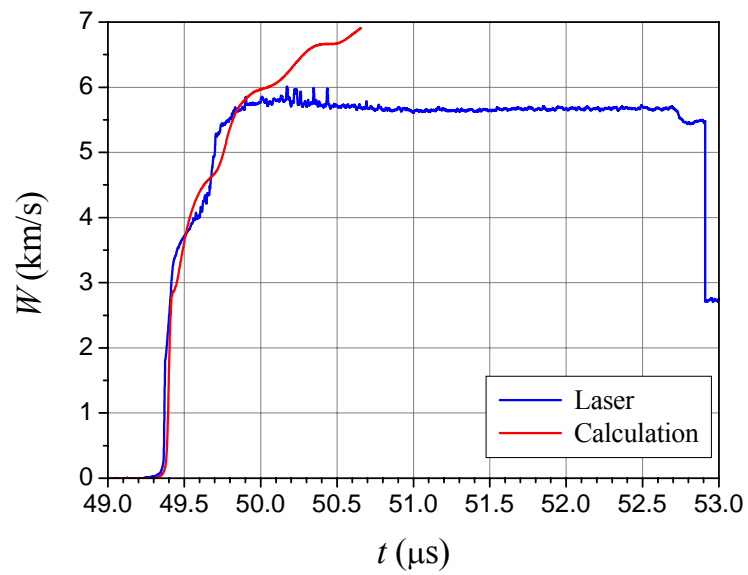


Fig. 5.5 - Experimental and calculated dependencies of free surface velocity on time  $W(t)$ .  
Liner thickness  $\Delta=1.78$  mm. Test №3

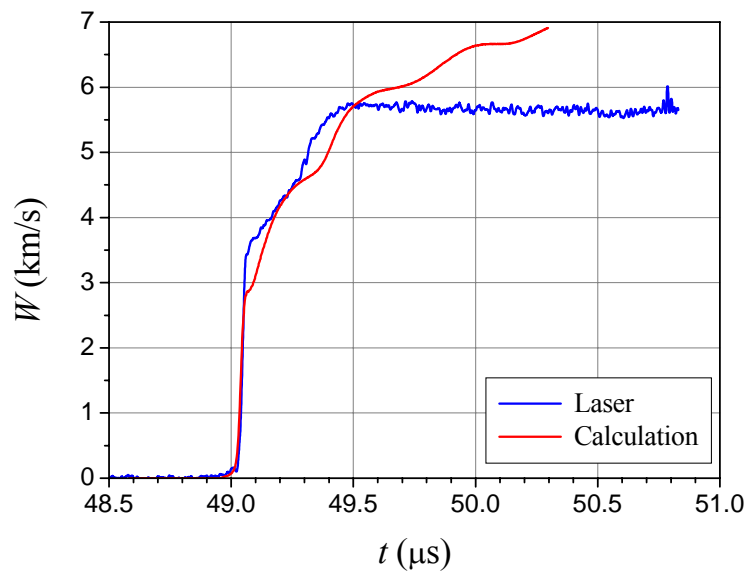


Fig. 5.6 - Experimental and calculated dependencies of free surface velocity on time  $W(t)$ .  
Liner thickness  $\Delta=1.78$  mm. Test №4

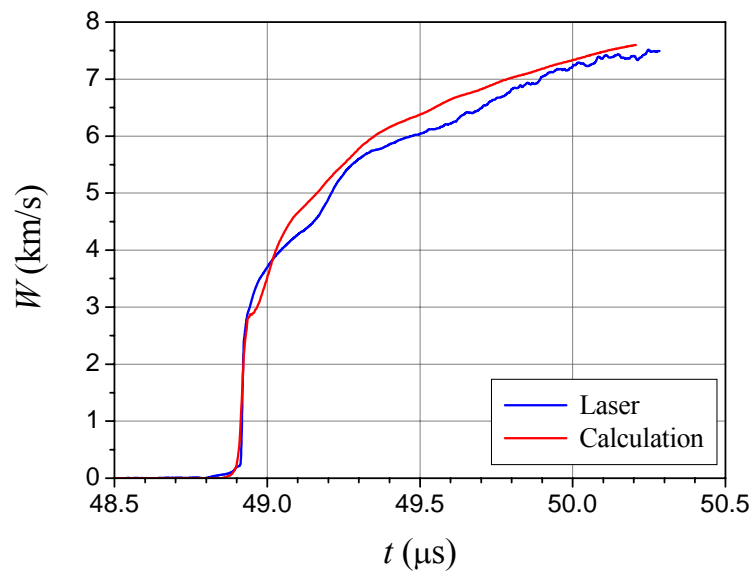


Fig. 5.7 - Experimental and calculated dependencies of free surface velocity on time  $W(t)$ .  
Liner thickness  $\Delta=1.78$  mm. Test №5

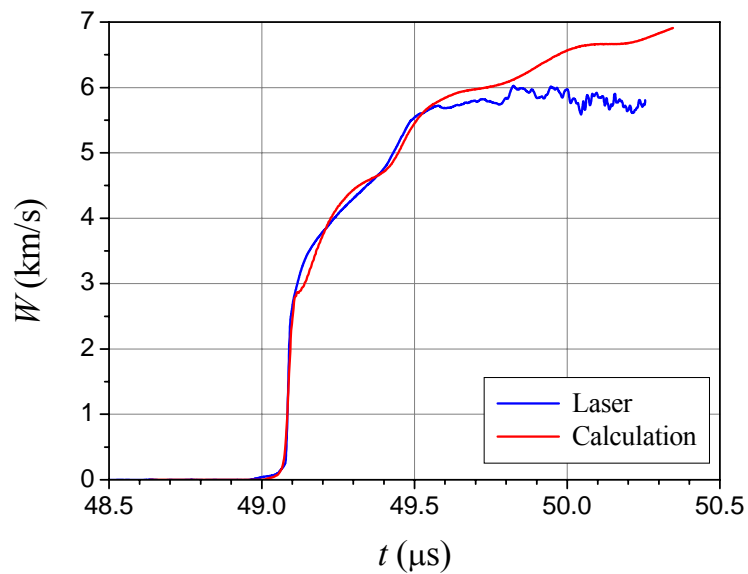


Fig. 5.8 - Experimental and calculated dependencies of free surface velocity on time  $W(t)$ .  
Liner thickness  $\Delta=1.78$  mm. Test №6

As is seen from Fig. 5.3 - Fig. 5.8, the calculating curve describes the experimental curve with the amplitude  $W$  within  $\sim 0.5 \mu\text{s}$  from a start of motion of FS, there are some divergences for the later times. The calculated value of a free surface velocity coincides with the calculated value in amplitude for test №5, however, there are some differences in sudden changes of acceleration as well.

It should be noted that in the time of basic loading of samples  $\Delta t \approx 0.5 \mu\text{s}$  calculated and experimental dependencies  $W(t)$ , are closely related to one another, what testifies to correctness of calculations of pressure at a beryllium surface and to repeatability of experiments.

Fig. 5.9 shows the experimentally measured pressure profiles and the calculated pressure profiles of manganin-based sensors  $D1$  and  $D2$  in test №1.

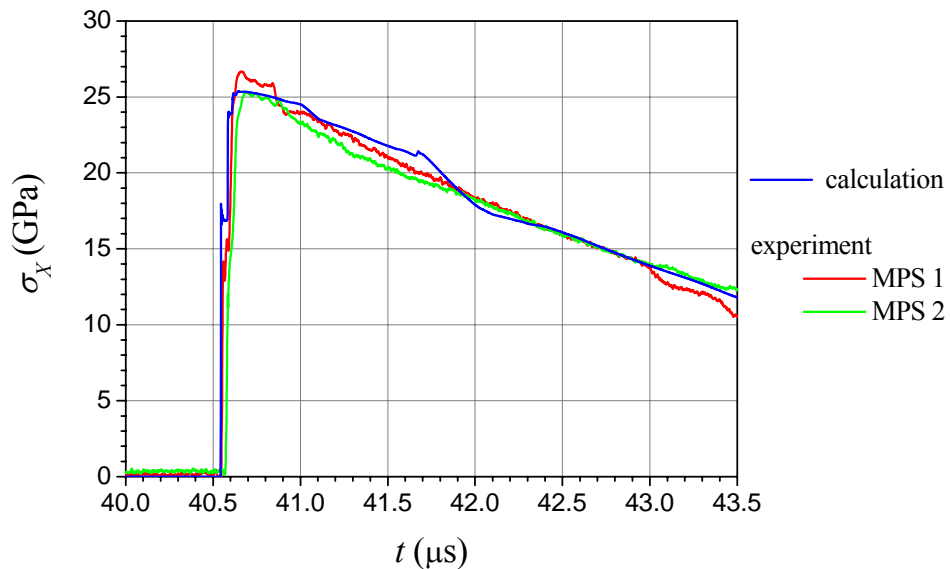


Fig. 5.9 – Pressure profiles. Test № 1

It is seen from Fig. 5.9 that shock wave amplitude coming from the aluminum disk, accounted for  $P_{\text{sw}} \approx 25 \text{ GPa}$ , the calculated curve is closely related to the experimental curve in this case.



Fig. 5.10 presents the experimentally measured pressure profiles and the calculated pressure profiles of manganin-based sensors *D1* and *D2* in test №2

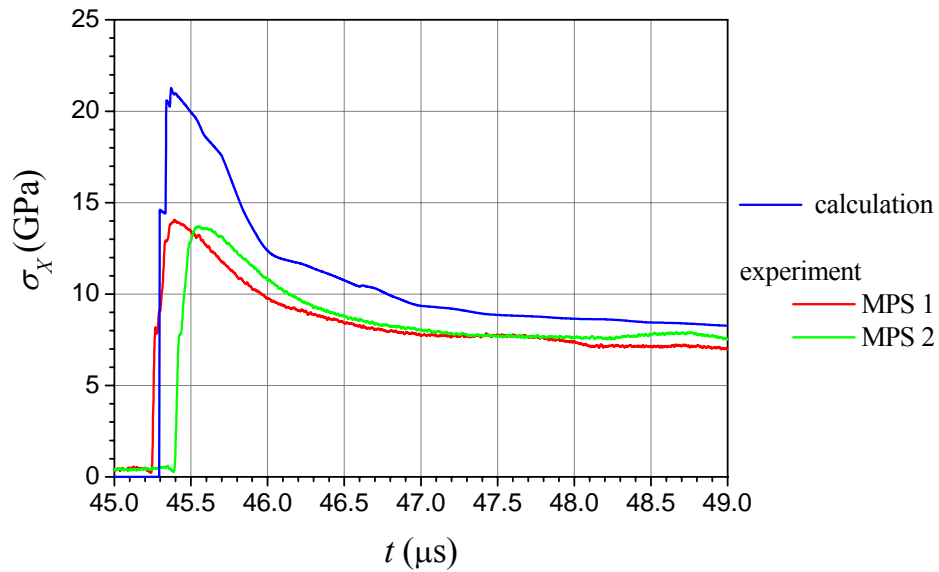


Fig. 5.10 – Pressure profiles. Test № 2

It is obvious from Fig. 5.10 that the calculated amplitude of the shock wave leaving the aluminum disk, amounted to  $P_{sw} \approx 21.5$  GPa and differs from the experimentally measured amplitudes  $P_{sw} \approx 14$  GPa.

A possible reason of such a large difference of experimental measurements from calculations consists in imperfection of equations of state of beryllium and rheological properties of beryllium. Other reasons exist also, for example, gaps between beryllium disks and aluminum disks.

## 6 Results of numerical simulation of experiments by using Lagrangian technique

The results of numerical simulation of the implemented experiments with the use of Lagrangian technique are presented in Fig. 6.1 and Fig. 6.2.

Dynamic strength models called RING were applied in calculations.

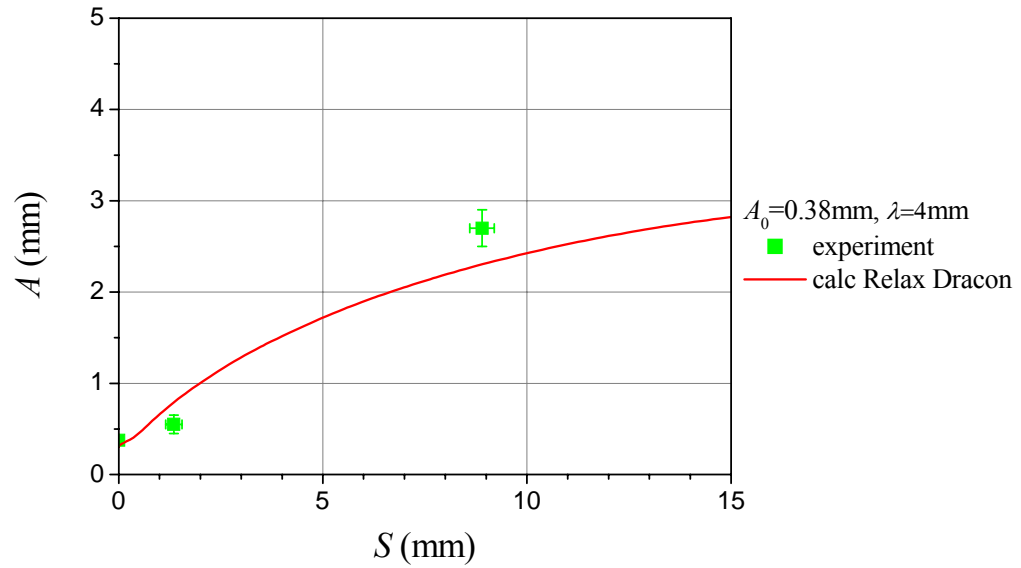


Fig. 6.1 - Experimental results and calculated dependencies of perturbation amplitudes on distance travelled by beryllium liner. Liner thickness  $\Delta=1.78$  mm

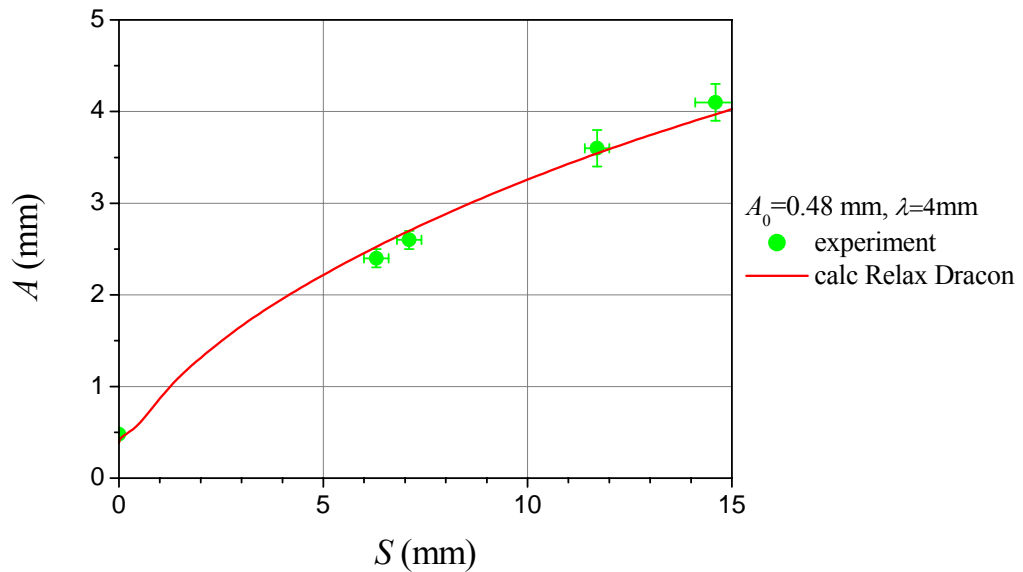


Fig. 6.2 - Experimental results and calculated dependencies of perturbation amplitudes on distance travelled by beryllium liner. Liner thickness  $\Delta=2.0$  mm

By analyzing the experimental results and numerical calculations, given in Fig. 6.1 - Fig. 6.2, the conclusion can be drawn that the authors manage to describe the majority of experimental results in calculations with the use of the RING dynamic strength model. Only one experiment can not be described with the liner thickness  $h=1.78$  mm and the amplitude  $A_0=0.38$  mm. It makes sense, apparently, to repeat experiments with the sample's thickness  $h=1.78$  mm with various initial perturbation amplitudes.

## **Conclusion**

The main results of the investigations performed in the framework of Contract B590737 are as follows:

The experts performed six roentgenographic experiments by using a dynamic method of perturbations with shock-free loading of the studied samples *Be S200F* up to the pressure  $P_m \approx 50$  GPa in the course of works at the third phase. Six values of amplitudes of perturbations were recorded. In addition, measurements of a free surface velocity of a beryllium liner of the *Be S200F* type were made in each experiment.

Two experiments were implemented with recovering beryllium samples after loading by pressure of  $P \sim 25 \div 60$  GPa and with a subsequent metallographic analysis. As a result of metallographic investigations the peculiarities of high-rate strain of *Be* were determined. The authors recorded the values of SW intensity using the methods of manganin-based pressure sensors.

Numerical simulation of experiments was performed using Eulerian and Lagrangian techniques. A relaxation model of dynamic strength called RING was used in the calculations for *Be S200F*. The majority of experiments were described adequately in the calculations. In one experiment the perturbation amplitude deviates from the calculated dependence by  $\approx 20\%$ , while a liner moves along the distance  $S \approx 9$  mm. Apparently, it is worth repeating the experiment with the same initial parameters, as well as it is necessary to carry out new experiments with smaller perturbation amplitude, which lies not far from a stability boundary of perturbations.

## **References**

---

- 1 A.I. Lebedev, P.N. Nizovtsev, V.A. Rayevsky, V.P. Soloviev.  
Rayleigh-Taylor Instability in Strong Media. Experimental Study.  
5<sup>th</sup> International workshop on the physics of compressible turbulent mixing. Stony Brook, New York, USA, 18-21 July, 1995, p. 231-236.
  
- 2 A.I. Lebedev, P.N. Nizovtsev, V.A. Rayevsky, V.P. Soloviev.  
Rayleigh-Taylor Instability in Strong Substances: Calculated Experimental Studies of instability in Titanium.  
6<sup>th</sup> International workshop on the physics of compressible turbulent mixing. Marseille. 1997, p. 307-311.
  
- 3 A.I. Lebedev, P.N. Nizovtsev, V.A. Raevsky.  
Rayleigh-Taylor instability in solids. 4-th International Workshop on the Physics of Compressible Turbulent Mixing.  
Cambridge, England, 29 March – 1 April 1993, pp. 81-93.
  
- 4 Lebedev A.I., Aprelkov O.N., Arinin V.A., Bulannikov A.S., Burtsev V.V., Golubev V.A., Davydov N.B., Zhernokletov M.V., Ignatova O.N., Igonin V.V., Makarov Yu.M., Manachkin S.F., Mochalov M.A., Nadezhin S.S., Nizovtsev P.N., Raevsky V.A., Sinitsyna S.N., Solov'ev V.P., Fadeev L.A.  
Perturbation Method for Study of Shear strength of Materials at Pressures up to ~300 GPa.  
*Shock Compression of Condensed Matter - 2005*. Proceedings of the Conference of the American Physical Society. Edited by M. D. Furnish, M. Elert, T.P. Russell, and C.T. White. American Institute of Physics. Baltimore, Maryland, July 31 - August 5, 2005. pp. 745-748.
  
- 5 V. A. Arinin and B. I. Tkachenko.  
Achieving the Ultimate Quality of Image Registration in Radiography.  
Pattern Recognition and Image Analysis, 2009, Vol. 19, No. 1, p. 63–68.

6 V. A. Arinin, B. I. Tkachenko.

Use of Abelian transformation for metrological aims when processing radiographic images. Proceedings of the International Conference XIII Khariton's Topical Scientific Readings «Extreme states of substance. Detonation. Shock waves». Sarov, 2011, p. 689-694.

7 V. A. Arinin.

Functional tracing of interfaces of two media in axisymmetric objects by using their X-ray photographs. International Conference «X Zababakhin's Readings », 15-19 April 2010, Snezhinsk, Chelyabinsk Region.

8 C.F. McMillan, D.R. Goosman et al.

Review of Scientific Instruments 59 (1988). № 1, 1-20.

9 T.I. Karmanova, B.G. Loboiko, A.T. Sapozhnikov, A.B. Syrtsov, V.V. Shaposhnikov, Wan Zeen Gtsy, Tsyn' Shiao Gan, Shi Shan Chwin. Calibration of manganin-based sensors for shock-wave studies. Chemical physics, 1998, V.17, №5, p.140-143.

10 V.I. Skokov, E.E. Lin, V.A. Medvedkin, S.A. Novikov.

About nature of shock load at dynamic compacting of ultra disperse diamonds. FGV, 1998, v.34, №3, p.105-106.

11 O.N. Aprelkov, V.V. Igonin, A.I. Lebedev, M.O. Lebedeva, V.A. Raevsky, A.M. Podurets et al.

Determination of dynamic strength of vanadium.

Report for Task 1 of Agreement № B539457 between LLNL and VNIIEF. 2006, 46 p.

- 12 O.N. Ignatova, V.A. Raevsky, S.S. Nadezhin.  
Development of constitutive relations of beryllium.  
Proceedings of the International Conference XIII Khariton's Topical Scientific Readings  
«Extreme states of substance. Detonation. Shock waves».  
Sarov, 2011, p. 184-185.
- 13 M.V. Zhernokletov, V.N. Zubarev, R.F. Trunin, V.E. Fortov.  
Experimental data on shock compressibility and adiabatic expansion of condensed  
substances at high energy densities.  
Chernogolovka, IKhFCh, 1996, 386 p.
- 14 Chhabildas L.C., Wise J.L., Asay J.R.  
Reshock and release behavior of beryllium.  
Shock Waves in Condensed Matter, 1981, California, p 422-426.
- 15 Physical values.  
Reference book under edition of I.S. Grigorieva, E.Z. Meilikhova.  
Moscow, Energoatomizdat, 1991.
- 16 L.V. Al'tshuler, S.E. Brusnikin.  
Equation of state of compressed and heated metals.  
TVT. # 1. 1987. P. 42-51.
- 17 L.V. Al'tshuler, S.E. Brusnikin, E.A. Kuzmenkov.  
Isotherms and functions of Grueneisen for 25 metals.  
PMTF, #1, 1987, p. 134-146.
- 18 Physical values.  
Reference book under edition of I.S. Grigorieva, E.Z. Meilikhova.  
Moscow, Energoatomizdat, 1991.
- 19 C. Deeney.  
Dynamic materials experiments on Z in support of Campaigns 2.1 and 2.2.  
CEGSNL Working Groups (2006).
-

20 Ph. Legrand and G. Robert.

First-principles thermoelasticity of beryllium.

Shock Compression of Condensed Mater. 2009, p. 513-516.

21 Tom Mehlhorn.

Overview of Sandia High Energy Density Physics Program.

Zababakhin Scientific Talks Snezhinsk.

Chelyabinsk Region, Russia 10-14 September, 2007.

22 S.K. Godunov, B.I. Romensky.

Non-stationary equations of nonlinear theory of elasticity in Eulerian coordinates. PMTF. # 6. 1972, p. 124-144.

23 W.R. Blumenthal, S.P. Abeln, D.D. Cannon, G.T. Gray III, R.W. Carpenter.

Influence of strain rate and temperature on the mechanical behavior of beryllium.

Shock Compression of Condensed Matter, 1997, p. 411-414.

24 J.W. Swegle and D.E. Grady.

J. Appl. Phys. 58, 692 (1985).

25 Dennis E. Grady.

Structured shock waves and the fourth-power law.

Journal of Applied Physics. Vol. 107, 2010, 013506, p. 1-13.

26 O.N. Aprelkov, V.V. Igonin, A.I. Lebedev, M.O. Lebedeva, V.A. Raevsky, A.M. Podurets et al.

Vanadium dynamic strength measurements.

Report on Phase 1 of Agreement # № B590737 between LLNL and VNIIEF.

2011, 71 p.

27 B.L. Glushak, O.N. Ignatova, S.S. Nadezhin, V.A. Raevsky

Relaxation model of shear strength of five metals (aluminum, beryllium, copper, tantalum, uranium)

VANT, ser. Mathematical simulation of physical processes.

2012, iss.2, p. 25-36.